

# On the Effectiveness of Persistent Homology

**Renata Turkeš**

University of Antwerp  
renata.turkes@uantwerpen.be

**Guido Montúfar**

University of California, Los Angeles  
montufar@math.ucla.edu

**Nina Otter**

Queen Mary University of London  
n.otter@qmul.ac.uk

## Abstract

Persistent homology (PH) is one of the most popular methods in Topological Data Analysis. Even though PH has been used in many different types of applications, the reasons behind its success remain elusive; in particular, it is not known for which classes of problems it is most effective, or to what extent it can detect geometric or topological features. The goal of this work is to identify some types of problems where PH performs well or even better than other methods in data analysis. We consider three fundamental shape analysis tasks: the detection of the number of holes, curvature and convexity from 2D and 3D point clouds sampled from shapes. Experiments demonstrate that PH is successful in these tasks, outperforming several baselines, including PointNet, an architecture inspired precisely by the properties of point clouds. In addition, we observe that PH remains effective for limited computational resources and limited training data, as well as out-of-distribution test data, including various data transformations and noise. For convexity detection, we provide a theoretical guarantee that PH is effective for this task, and demonstrate the detection of a convexity measure on the FLAVIA dataset of plant leaf images.

## 1 Introduction

Persistent homology (PH) is an extension of homology, which gives a way to capture topological information about connectivity and holes in a geometric object. PH can be regarded as a framework to compute representations of raw data that can be used for further processing or as inputs to learning algorithms. There are numerous successful applications of PH in the last decade, from prediction of biomolecular properties [19, 18, 101], face, gait and activity recognition [112, 58, 62, 52] or digital forensics [6], to discriminating breast cancer subtypes [89], quantifying the porosity of nanoporous materials [61], classifying fingerprints [46], or studying the morphology of leaves [63].<sup>1</sup> At the same time, the reasons behind these successes are not well understood. Indeed, the data used in real-world applications is complex, so that there are numerous effects at play and one is often left unsure why PH worked, i.e., what type of topological and/or geometric information it captured that facilitated the good performance. The goal of this work is to shed some light on this issue, by identifying some fundamental classes of problems suitable for PH.

Here we investigate *what* is seen by persistent homology: Given a data set, i.e., a point cloud, which underlying topological and geometric features can we detect with PH? This question is related to manifold learning and, specifically, topological and geometric inference: Given a finite point cloud  $X$  of (noisy) samples from an unknown manifold  $M$ , how can one infer properties of  $M$  [24, 27, 12, 11]? Obtaining a representation of a shape that can be used in statistical models is an important task in data analysis and numerous approaches to modeling surfaces and shapes [96].

Since PH is inspired by homology, which provides a measure for the number of connected components, holes, voids, and higher-dimensional cycles of a space — to which we collectively refer as “topological features” —, we start with the obvious question of whether PH applied to a point cloud sampled from a geometric object can detect the *number of (1-dimensional) holes* of the underlying object. Unlike homology, however, PH registers also the persistence of topological features across scales,

<sup>1</sup>A database of applications of persistent homology is being maintained at [47].

and can thereby capture geometric information, such as size or position of holes. We therefore also investigate how well PH can detect fundamental geometric notions as are *curvature* and *convexity*. To gauge the performance of PH, we compare it against several baselines. As a first machine learning (ML) baseline we take an SVM trained on the distance matrices of point clouds. We further consider fully-connected neural networks (NN) with a single or multiple hidden layers, also trained on distance matrices. As a stronger baseline we consider a PointNet trained on the point clouds directly. PointNet [79, 1] is designed specifically for point cloud data. Similar architectures with convolutional (and fully-connected and pooling) layers have been applied for Betti-number and curvature estimation [73, 48].

**Related works** In spite of the growing interest in PH, so far there is only limited work in the direction that we pursue here. There is indeed theoretical evidence that the number of holes of the underlying space can be detected from PH (under some conditions about the target space, the sample density and closeness to the space) [30, 69, 56], and there is significant interest in investigating how well this works in practice [28]. However, so far there are only few available results. Some works demonstrate that PH can be used to detect the number of holes, but only on individual toy examples (e.g. [24, Figure 19], [27, Figures 2, 3, 6, 11, 12], [81], without looking into the statistical significance between different classes of data, or the accuracy of some classification algorithms on a comprehensive dataset. In [19], PH is estimated for large dataset of point clouds, but with the goal of using this information to study the behaviour of deep neural networks, so that the soundness of this estimation is not investigated, what is the focus of our work.

Some insights about PH and curvature have been obtained in the literature, starting with an illustrative example in [36, Figure 12] which shows that PH on the filtered tangent complex can distinguish between letters (C and I) that have the same topology, since their curvature is different. Recently, [17] show both theoretically and experimentally that PH can predict curvature (with computational experiments replicated in [99]), which inspired us to investigate this problem in more detail.

Regarding the important geometric problem of classification between convex and concave shapes, we were not able to identify any previous works investigating the applicability of PH to this task.

Some further recent work investigating the topological and geometric features seen by PH are the following. Bubenik and Dłotko [16] show that using PH of points sampled from spheres one can determine the dimension of the underlying spheres. A connection has also been established between PH and the magnitude of a metric space (an isometric invariant) [71]. There have been several efforts in using PH to estimate fractal dimensions, such as [86] in which Schweinhart proves that the fractal dimension of some metric spaces can be recovered from the PH of random samples.

**Main contributions** Our contributions can be summarized as follows.

- We prove that PH can detect convexity (Theorem 1).
- We demonstrate experimentally that PH can detect the number of holes (Section 3), curvature (Section 4), and convexity (Section 5) from synthetic point clouds in  $\mathbb{R}^2$  or  $\mathbb{R}^3$ , outperforming SVMs and fully-connected networks trained on distance matrices, and PointNet trained on point clouds. For convexity detection, we also show the effectiveness of PH on a real-world dataset of plant leaf images.
- We demonstrate experimentally that PH features allow to solve the above tasks even in the case of limited training data (Section 3), noisy (Section 3) and out-of-distribution (Section 5) test data, and limited computational resources (Section 3, Section 4, Section 5).
- We provide insights about the topological and geometric features that are captured with long and short persistence intervals (Section 6), and formulate guidelines for applications that are suitable for PH (Section 7).
- We provide data sets that can be directly used as a benchmark for our tasks or other related point-cloud-analysis or classification problems. We provide computer code to construct more data and replicate our experiments.

## 2 Background on persistent homology

Homology is a topological concept that attempts to distinguish between topological spaces by constructing algebraic invariants that reflect their connectivity properties [81], i.e.,  $k$ -dimensional cycles (connected components, holes, voids, ...). The number of independent  $k$ -dimensional cycles is called  $k$ -th Betti number and denoted by  $\beta_k$ . For example, the circle has Betti numbers  $\beta_0 = 1$ ,  $\beta_1 = 1$ ,  $\beta_2 = 0$ , and for a torus, we have  $\beta_0 = 1$ ,  $\beta_1 = 2$ ,  $\beta_2 = 1$ .

Persistent homology is an extension of this idea [113] that has found success in applications to data. To calculate PH from some data  $X$ , we must first build a filtration, i.e., a family of topological spaces  $K_1 \subseteq K_2 \subseteq \dots K_r \subseteq \dots K_k$  which, in a suitable sense, approximate  $X$  at different scales  $r \in \mathbb{R}$ . Typically,  $X = \{\mathbf{x}_1, \mathbf{x}_2, \dots, \mathbf{x}_n\}$  is a point cloud in  $\mathbb{R}^d$ , and  $K_r$  is a simplicial complex, a set of simplices  $\sigma$  (which we can think of as vertices, edges, triangles, ...) such that if  $\sigma \in K_r$  and  $\tau \subseteq \sigma$ , then  $\tau \in K_r$  [36]. A common choice is  $K_r = VR(X, r)$ , where  $VR(X, r)$  is the Vietoris-Rips simplicial complex, in which  $\sigma = \{\mathbf{x}_1, \dots, \mathbf{x}_n\} \in VR(X, r)$  when  $d(\mathbf{x}_i, \mathbf{x}_j) \leq r$  for all  $1 \leq i, j \leq n$ . PH can then be summarized with a persistence diagram (PD), a scatter plot with the  $x$  and  $y$  axes respectively depicting the scale  $r \in \mathbb{R}$  at which each cycle is born and dies or is identified (i.e., merges) with another cycle within a filtration. The length  $l = d - b$  of a persistence interval  $(b, d)$  measures the lifespan — the so-called “persistence” — of the corresponding cycle in the filtration.

Instead of working directly with persistence diagrams, these are often represented by other signatures that are better suited for machine learning frameworks. A common choice is a persistence image (PI) [2] (discretized sum of Gaussian kernels centered at the PD points), or a persistence landscape (PL) (functions obtained by “stacking isosceles triangles” above persistence intervals, with height reflecting their lifespan) [15]. The steps for extracting PH features are visualized in Appendix B.2. For good choices of filtration and signature [95], there are theoretical results that guarantee that PH is stable under small perturbations [25, 90]. After the PH signature is calculated, statistical hypothesis testing [15, 10], or machine learning techniques such as SVM or k-NN [2, 44, 70] can be used on these features to study the differences within the dataset of interest.

It is important to note that PH is very flexible, as different choices can be made in every step of the pipeline, regarding the input and output of PH, as detailed in the remainder of this section.

### 2.1 Approximation of a space at scale $r \in \mathbb{R}$

Instead of the Vietoris-Rips complex, other types of complexes can be used to approximate the data  $X$  at the given scale  $r \in \mathbb{R}$ . For instance, since Vietoris-Rips simplicial complex is computationally expensive [72], one might rather choose the alpha complex [42] (for a visualization, see Appendix C), which is closely related to the Vietoris-Rips complex [56], but consists of significantly less simplices and is faster to construct [72, Table 1] when the dimension of the ambient space is 2 or 3. If data  $X$  is an image rather than a point cloud, or if the point cloud can be seen as an image without losing important information, cubical complexes [53] might be a more suitable choice, where vertices, edges and triangles are replaced by vertices, edges and squares (for a visualization, see Appendix E).

### 2.2 Filtration

A filtration  $K_1 \subseteq K_2 \subseteq \dots K_r \subseteq \dots K_k$  of a point cloud in  $\mathbb{R}^d$  can be constructed from any function  $f : \mathbb{R}^d \rightarrow \mathbb{R}$  by considering  $K_r$  to be the sublevel set of  $f$  thresholded by  $r \in \mathbb{R}$ :  $\{\mathbf{y} \in \mathbb{R}^d \mid f(\mathbf{y}) \leq r\}$ . The underlying filtration function in the common PH pipeline introduced above is the distance function  $\delta_X : \mathbb{R}^d \rightarrow \mathbb{R}$ , where  $\delta_X(\mathbf{y}) = \min\{d(\mathbf{y}, \mathbf{x}) \mid \mathbf{x} \in X\}$  is the distance to point cloud  $X$ . Indeed, the Vietoris-Rips simplicial complex  $VR(X, r)$  approximates the sublevel set

$$K_r = \delta_X^{-1}((-\infty, r]) = \{\mathbf{y} \in \mathbb{R}^d \mid \delta_X(\mathbf{y}) \leq r\} = \cup_{\mathbf{x} \in X} B(\mathbf{x}, r),$$

where  $B(\mathbf{x}, r)$  is a ball with radius  $r$  centered around  $\mathbf{x} \in X$  [26].

However, PH on such a filtration is very sensitive to outliers, since even a single outlier changes  $\delta_X$  significantly. In the presence of outliers, it is better to replace the distance function with the Distance-to-Measure (DTM)  $\delta_{X,m} : \mathbb{R}^d \rightarrow \mathbb{R}$ , where  $\delta_{X,m}(x)$  is the average distance from a number of neighbors on the point cloud [26, 5] (for a visualization, see Appendix C). However, depending on the task, there are many other filtration functions one could choose, such as rank [75], height, radial,

erosion, dilation [44], and the resulting PH captures completely different information about the cycles [95]. For example, whereas PH with respect to the Vietoris-Rips filtration encodes the size of the hole (for a visualization, see Appendix B.2), PH on the height filtration informs about the position of the hole (Appendix E). For a more detailed discussion about the influence of filtration, see Appendix F.

### 2.3 Persistence signature

Next to PIs and PLs, a plethora of persistence signatures has been introduced in the literature, e.g., Betti numbers [51, 98] or Euler characteristic [64] (across scales), or even scalar summaries such as amplitude [44], entropy [32, 84], or algebraic functions of the birth and death values [4, 55]. Some of these signatures summarize the same information, but lie in different metric spaces [97]. Others, however, such as the scalar summaries listed above, discard information compared to PDs, as it might sometimes be useful to, e.g., only capture the (total or maximum) persistence of intervals, but not all the detailed information about all birth and death values (see Appendix F).

## 3 Number of holes

In this section, we focus on the task of (ordinal) classification of point clouds by the number of 1-dimensional holes. Research in psychology shows that global properties often dominate perception, and, in particular, that topological invariants such as number of holes, inside versus outside, and connectivity can be effective primitives for recognizing shapes [76]. Extracting such topological information can therefore prove useful for many computer vision tasks. There are theoretical results in the literature that ensure that PH with respect to the alpha simplicial complex can be successful for this problem (Appendix A), and the computational experiments that follow demonstrate this success in practice.

**Data** We consider 20 different shapes in  $\mathbb{R}^2$  and  $\mathbb{R}^3$ , with four different shapes having the same number of holes (0, 1, 2, 4 or 9). For each shape, we construct 50 point clouds each consisting of 1 000 points sampled from a uniform distribution over the shape, resulting in a balanced dataset of  $1\,000 = 20 \times 50$  point clouds. A few examples of these point clouds are shown in Figure 1. The label of a point cloud is the number of holes in the underlying shape.

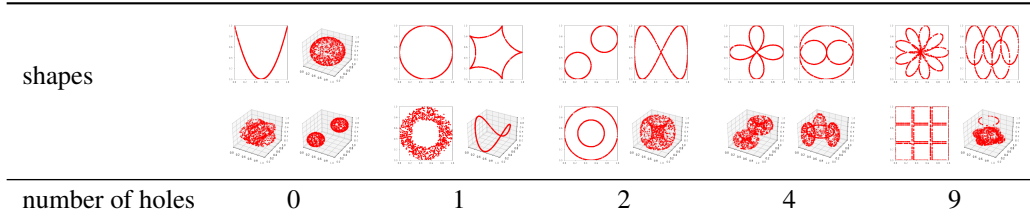


Figure 1: Number of holes dataset.

**PH pipeline** For each point cloud  $X$  and scale  $r \in \mathbb{R}$ , we consider its alpha complex. We will look into scenarios in which data contains noise, and therefore, instead of the standard distance function, we consider Distance-to-Measure (DTM) as the filtration function. We extract 1-dimensional PDs, that are then transformed to PIs, PLs, or a simple signature consisting only of lifespans  $l = d - b$  of the 10 most persisting cycles (as there are at maximum 9 holes of interest in the given dataset)<sup>2</sup>, and classified with an SVM. We consider a “PH simple” pipeline, which relies on the 10 lifespans, and a “PH” pipeline wherein grid search is employed to choose the best out of the three aforementioned persistent signatures and the values of their parameters. For more details on the pipeline, see Appendix B and Appendix C.

**Results** We investigate the clean and robust test accuracy under four types of transformations (translation, rotation, stretch, shear) and two types of noise (Gaussian noise, outliers). For more details

<sup>2</sup>Although a sphere has no 1-dimensional holes, its PD might consist of many short intervals which correspond to the small holes on the surface. In addition, in the presence of noise, additional small holes might appear for any point cloud. Hence it is not a good idea to consider the cardinality  $|\text{PD}|$  of the PD as the signature.

on these transformations, see Appendix C. We train the classifier on 80% of the original point clouds, and test on the remaining 20% of the data either in its original form or subject to transformations and noise. The results reported in Figure 2 show that PH obtains very good test accuracy on this classification task, even in the presence of affine transformations or noise, outperforming baseline machine- and deep-learning techniques.<sup>3</sup>

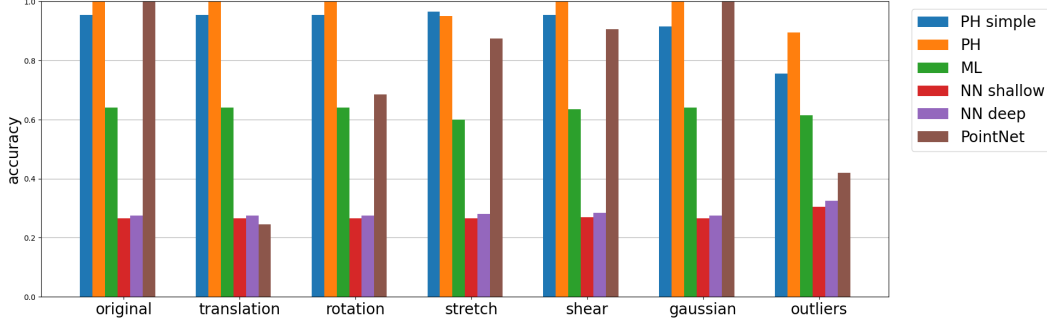


Figure 2: Persistent homology can detect the number of holes.

We reach a similar conclusion in case of limited training data and computational resources (Appendix C). Firstly, the evolution of the test accuracy across different amounts of training data demonstrates that PH achieves good performance for a small number of training point clouds, which is not the case for other pipelines. Secondly, although the hyperparameter tuning of the PH pipeline does take time (as we consider a wide range of parameters for the different persistence signatures), it is still less than for PointNet. Moreover, Figure 2 shows that even the simple PH pipeline, where the SVM is used directly on the lifespans of the 10 most persisting cycles (without any tuning of PH-related parameters) performs well.

## 4 Curvature

This section considers a regression task to predict the curvature of an underlying shape based on a point cloud sample. Estimating curvature-related quantities is of prime importance in computer vision, computer graphics, computer-aided design or computational geometry, e.g., for surface segmentation, surface smoothing or denoising, surface reconstruction, and shape design [23]. For continuous surfaces, normals and curvature are fundamental geometric notions which uniquely characterize local geometry up to rigid transformations [48]. Recently, it has been shown that, using PH, curvature can be both recovered in theory (Appendix A), and effectively estimated in practice [17]. We run a similar experiment, evaluating the PH pipeline against our baselines, and also taking a closer look into the importance of short intervals.

**Data** A balanced dataset is generated in the same way as in [17]: We consider unit disks  $D_K$  on surfaces of constant curvature  $K$ : (i)  $K = 0$ , Euclidean plane, (ii)  $K > 0$ , sphere with radius  $1/\sqrt{K}$ , and (iii)  $K < 0$ , Poincaré disk model of the hyperbolic plane (surface of a saddle, or a potato chip). Curvature  $K$  lies in the interval  $[-2, 2]$  so that a disk with radius one can be embedded on the upper hemisphere of a sphere with constant curvature  $K$  (as its spherical cap). For each  $K \in \{-2, -1.96, \dots, -0.04, 0, 0.04, \dots, 1.96\}$ , we construct 10 point clouds by sampling 1000 points from the unit disk  $D_K$  with the probability measure proportional to the surface area measure [15, Section 2.7, Section 4.1]. A few examples are illustrated in Figure 3. These  $101 \times 10 = 1010$  point clouds are considered as the training data, whereas the test dataset is built in a similar way for

<sup>3</sup>Interestingly, although PointNet was designed with the idea to be invariant to affine transformations, it performs poorly when the test data is translated or rotated (and this is consistent with some previous results [108, 107, 60, 106, 109, 102, 110]), or when it contains outliers. Traditional neural networks perform very poorly, which might not come as a big surprise, since it was recently demonstrated that they transform topologically complicated data into topologically simple one as it passes through the layers, vastly reducing the Betti numbers (nearly always even reducing to their lowest possible values:  $\beta_k = 0$  for  $k > 0$ , and  $\beta_0 = 1$ ) [68]. Of course, the choice of activation function and hyperparameters might have an important influence on performance [68].

100 values of  $K$  chosen uniformly at random from  $[-2, 2]$ . The label of a point cloud is the curvature  $K$  of the underlying disk  $D_K$ . Note that all these disks are homoeomorphic: they are contractible, so that their homology is trivial and homology is thus unable to distinguish between them [17].

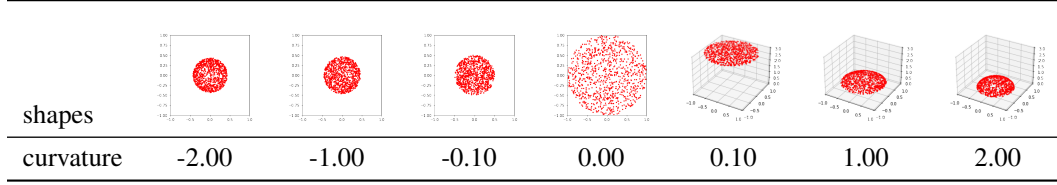


Figure 3: Curvature dataset.

**PH pipeline** For each point cloud  $X$ , we first calculate the suitable matrix of pairwise distances between the point-cloud points: hyperbolic, Euclidean or spherical, respectively for negative, zero and positive curvature [15, Section 2.7]. The input for PH is the filtered Vietoris-Rips simplicial complex.<sup>4</sup> We extract 0- and 1-dimensional PDs, which are then transformed into PIs, PLs or lifespans, to be fed to SVM. This PH pipeline is visualized in Appendix D.

**Results** Figure 4 shows the mean squared errors for the PH and other pipelines, together with their regression lines. The results show that PH indeed detects curvature, outperforming other methods.<sup>5</sup> Next to the PH pipeline discussed above, wherein a grid search is used to tune the parameters (Appendix B), we also consider SVM on the lists of lifespans of all persistence intervals (PH simple), and SVM only on the 10 longest lifespans (PH simple 10), in order to investigate if all persistence intervals contribute to prediction. We see that the performance drops if we only focus on the longest 10 intervals, so that the many short intervals together capture the geometry of interest for this problem.

Similarly as in Section 3, the grid search across the different parameters for persistence signatures does take time (Appendix D), but Figure 4 shows that SVM on a simple signature of all (0-dimensional) lifespans performs well.

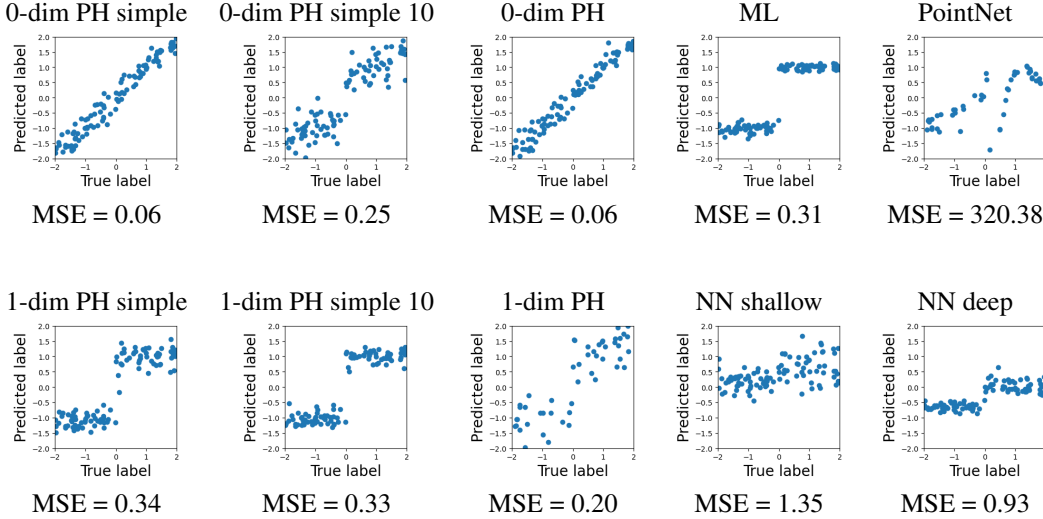


Figure 4: Persistent homology can detect curvature.

<sup>4</sup>Alpha complex is faster to compute, but requires information about the position, i.e., the coordinates of the points and therefore cannot be calculated on a distance matrix. To calculate PH, we rely on the Ripser software [94], which is at the time the most efficient library to compute PH with Vietoris-Rips complex [72].

<sup>5</sup>Simple machine and deep learning techniques are able to differentiate between positive and negative curvature, but perform poorly in predicting the actual value of the curvature of the underlying surface.

We highlight that the data used here, as was the data in Bubenik’s work [17], is sampled from surfaces with *constant* curvature. In future work it would be interesting to conduct similar experiments on shapes with non-constant curvature.

## 5 Convexity

In this section, we consider the binary classification task that consists in detecting whether a point cloud is sampled from a convex set. Convexity is a fundamental concept in geometry [37], which plays an important role in learning, optimization [9], numerical analysis, statistics, information theory, and economics [82]. Furthermore, points of convexities and concavities have been demonstrated as crucial for human perception of shapes across many experiments [85].

To the best of our knowledge, prior to our work PH has not been employed to analyze convexity, and it is a task for which PH’s effectiveness might seem surprising. In the first decade after the introduction of PH, it was seen primarily as the descriptor of global topology. Recently, there have been many discussions and greater understanding that PH also captures local geometry [3]. However, it is still suggested that the long persistence intervals capture topology (as was the case with the detection of holes in Section 3), and many—even too many for the human eye to count—short persistence intervals capture geometrical properties (as was the case with curvature prediction in Section 4). However, as we show in the following theorem (proof in Appendix A) and as our experiments suggest, it is a single, and the second-longest persistence interval that enables us to detect concavity.

**Theorem 1.** *Let  $X \subset \mathbb{R}^2$  be triangulable. Let  $\ell$  be any line in  $\mathbb{R}^2$ , and denote by  $h_\ell$  the height function with respect to  $\ell$ . For any  $r \in \mathbb{R}_{\geq 0}$ , denote by  $X_{h_\ell, r}$  the subset of points at distance at most  $r$  from  $\ell$ . Then  $X$  is convex if and only if the persistence diagram in degree 0 of the filtered space  $\{X_{h_\ell, r}\}_{r \in \mathbb{R}_{\geq 0}}$  contains exactly one interval.*

**Data** We construct a balanced dataset of 1 000 point clouds by sampling 5 000 points from convex and concave (nonconvex) shapes in  $\mathbb{R}^2$ . First, we consider the “regular” convex shapes of triangle, square, pentagon and circle, and their concave variants, sampling 60 point clouds of each of the eight shapes, 480 point clouds in total. Next, we build 480 “random” convex and concave shapes, in order to be able to investigate if an algorithm is actually detecting convexity, or only the different basic shapes. A few examples are shown in Figure 5. To construct a random convex shape, we generate 10 points at random, and then build their convex hull using the quickhull algorithm [100]. We construct random concave shapes in a similar way, but instead of the convex hull, we build the alpha shape [41, 43] with the optimized  $\alpha$  parameter, which gives a finer approximation of a shape from a given set of points. If the alpha shape is convex (i.e., if the alpha shape and its convex hull are the same), we reconstruct the concave shape from scratch. A point cloud has label 1 if it is sampled from a convex shape, and 0 otherwise.

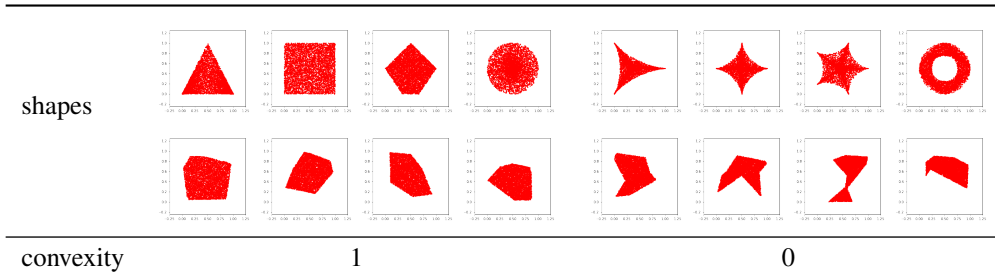


Figure 5: Convexity dataset.

**PH pipeline** To build a filtration, we consider cubical complexes filtered by height functions that measure the distance of points from a certain line, see Appendix A for a precise definition. For a good choice of line, multiple connected components would be seen in the filtration of a point cloud sampled from a concave shape, at least for some values  $r \in \mathbb{R}$  (see also the illustrations in Figure 7(a) in the Appendix). For this reason we consider the cubical complex, rather than the standard Vietoris-Rips simplicial complex wherein these separate components would commonly be connected with an edge.

To build an image from the point cloud, we define a pixel as black if it contains any point-cloud points, and white otherwise.

Since sources of concavity can lie anywhere on the point cloud, we consider nine different directions for the height filtration function (for a visualization of the pipeline, see Appendix E). For each of the nine directions, we extract 0-dimensional PD, as it captures information about the connected components. If the point cloud is thus sampled from a convex shape, its PD will only see a single cycle from any direction, whereas there will be multiple cycles at least for some direction for points clouds sampled from concave shapes. For this reason, for each of the nine directions, we focus our attention only on the lifespan of the second most persisting cycle. We can consider this 9-dimensional vector as our PH signature, but in our experiment choose an even simpler summary: the maximum of these lifespans, since we only care if there are multiple connected components *from at least one direction*. This scalar could even be used as some measure of a level of concavity of a shape.

**Results** As already indicated, to gain some insights into how well the different approaches discriminate convexity from concavity rather than differentiating between the different basic shapes, we look at the classification accuracies under different conditions (Figure 6). We start with the easiest case, where both the train and test data consist of the simple regular convex and concave shapes (Figure 5, first row), and then proceed to the scenario where both train and test data are random shapes (Figure 5, second row). Next we proceed to out-of-distribution test data, where we train on the regular and test on random shapes, or vice versa. In every case, we train on 400 and test on 80 point clouds. The results show that PH is able to detect convexity, surpassing other methods significantly in all scenarios except for PointNet in the scenario on the dataset of regular shapes which performs on par. Results reported in Appendix E show PH is also computationally efficient.

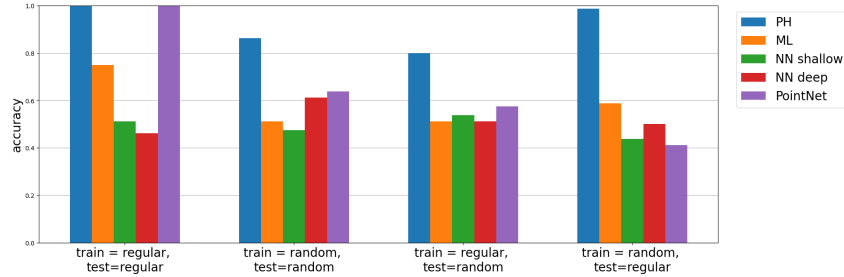


Figure 6: Persistent homology can detect convexity.

The PH pipeline above makes a wrong prediction when concavity is barely pronounced, or if it is missed by the selected height filtration directions (for details see Appendix E). However, the accuracy of PH can easily be improved simply by considering a finer resolution for the cubical complexes and/or additional height filtration directions (Appendix A). The particular PH pipeline summarized in this section would also make a wrong prediction if the dataset would include shapes that have small or non-central holes, e.g., a square with a hole in the top left corner. In this case, the accuracy could also be improved by considering a finer cubical complex resolution and by considering additional non-central height filtration directions within shapes, or by adding (the maximum lifespan of the) 1-dimensional PH which captures holes. The pipeline is not limited to polygons, or connected shapes, and it can be generalized to surfaces in higher dimensions (for a detailed discussion, see Appendix A.4).

In Appendix G, we also consider the real-world dataset FLAVIA for which we demonstrate that a PH pipeline is effective in detecting convexity.

## 6 Implications for PH interpretation: topology vs. geometry

Here we discuss how our results contribute to the important and ongoing discussion about the interpretation of long versus short persistence intervals. When PH was first introduced in the literature, the long intervals were commonly considered as important or “signal”, and short intervals as irrelevant or “noise” [35]. Subsequently the discussion has refined when it was shown that short and medium-length persistence intervals have the most distinguishing power for specific types of



applications [8, 91]. The current understanding is roughly that long intervals reflect the topological signal, and (many) short intervals can help in detecting geometric features [3]. We believe that our work brings new insight into this discussion. We give a summary of the implications of our work in this section, and we provide a more detailed discussion in Appendix F.

**Topology and long persistence** Stability results guarantee that a number of longest persistence intervals reflect the topological signal, i.e., the number of cycles [30]. These theorems give information about the threshold that differentiates between long and short persistence intervals. In Section 3, where we focus on the topology of underlying shapes, the experiments demonstrate that this threshold can be learned with simple machine learning techniques. However, it is important to highlight that the distinction between long and short persistence is vague in practice. Indeed, seemingly short persistence intervals capture the topology in Section 3, but the second-longest interval is topological noise in Section 5, since every shape in the dataset has only a single connected component (although this second-longest interval captures important *geometric* information, what enabled us to discriminate between convex and concave shapes). These two problems also clearly indicate how the long intervals that encode topology might or might not be irrelevant, depending on the signal of the particular application domain.

**Geometry and short persistence** The current understanding is that (many) short persistence intervals detect geometry. Section 4 confirms that this indeed can be the case. However, we highlight that *all* cycles can encode geometric information, such as the information about their size (with respect to the Vietoris-Rips and related filtrations, as in Sections 3 and 4) or their position (with respect to the height filtration, as in Section 5). This further implies that, depending on the application, *any number* of short or intervals of *any persistence* can be important, which was clearly demonstrated in Section 5, where we show that a single interval detects convexity.

## 7 Conclusions

**Main contribution** The goal of this work is to gain a better understanding of the topological and geometric features that can be captured with persistent homology. We focus on the detection of number of holes (Section 3), curvature (Section 4), and convexity (Section 5). Theoretical evidence for the first two classes of problems has been established in the literature, and we prove a new result that guarantees that PH can detect convexity (Theorem 1). We also experimentally demonstrate that PH can solve all three problems for synthetic point clouds in  $\mathbb{R}^2$  and  $\mathbb{R}^3$ , outperforming a few baselines. This is true even when there is limited training data and computational resources, and for noisy or out of distribution test data. For convexity detection, we also show the effectiveness of PH in a real world plant morphology application.

**Relevance** Firstly, the findings point the way to further advances in utilizing the potential of PH in applications: we can expect PH to be successful for classification or regression problems where the data classes differ with respect to number of holes, curvature and/or convexity. Detailed guidelines are discussed in Appendix F. Due to the crucial role of shape classification in understanding and recognizing physical structures and objects, image processing and computer vision [65], our results demonstrate that PH can—to borrow the words from Wigner [103]—“remain valid in future research, and extend, to our pleasure”, and lesser bafflement, to a variety of applications.

Secondly, the results advance the discussion about the importance of long and short persistence intervals, and their relationship to topology and geometry (Section 6). Topology is captured by the long intervals, geometry is encoded in all persistence intervals, and any interval can encode the signal in the particular application domain.

**Limitations** The results focus on three selected problems and datasets, and it would therefore be interesting to consider other tasks. In addition, we do not have an extensive comparison of the state-of-the-art for the given problems. Our work seeks to understand if PH is successful for a selected set of tasks by benchmarking it against some well-performing methods.

**Future research** An in-depth analysis of the hypothetical applications discussed in this paper (Appendix F) and selected success stories of PH from the literature could further improve our

understanding of the topological and geometric information encoded in PH, and the interpretation of persistence intervals of different lengths. The extension of PH for detection of convexity in higher dimensions is a particularly interesting avenue for further work. Furthermore, even though our results imply that PH features are recommended over baseline models for the three selected classes of problems, they also provide inspiration on how to improve existing learning architectures. Further work could investigate deep learning models on PH (and standard) features or kernels [50, 14, 80], an additional network layer for topological signatures, or PH-based priors, regularization or loss functions [14, 31, 34, 33, 111, 104].

**Potential negative societal impact** While we recognize that the applications of shape analysis can take many different directions, we do not foresee a direct path of this research to negative societal impacts.

**Funding transparency statement** This research was conducted while RT was a Fulbright Visiting Researcher at UCLA. GM acknowledges support from the European Research Council (ERC) under the European Union’s Horizon 2020 research and innovation programme (grant agreement n° 757983).

## References

- [1] Point cloud classification with PointNet. <https://keras.io/examples/vision/pointnet/>. Accessed: 2022-02-01.
- [2] Henry Adams, Tegan Emerson, Michael Kirby, Rachel Neville, Chris Peterson, Patrick Shipman, Sofya Chepushtanova, Eric Hanson, Francis Motta, and Lori Ziegelmeier. Persistence images: A stable vector representation of persistent homology. *The Journal of Machine Learning Research*, 18(1):218–252, 2017.
- [3] Henry Adams and Michael Moy. Topology applied to machine learning: From global to local. *Frontiers in Artificial Intelligence*, 4:54, 2021.
- [4] Aaron Adcock, Erik Carlsson, and Gunnar Carlsson. The ring of algebraic functions on persistence bar codes. *arXiv preprint arXiv:1304.0530*, 2013.
- [5] Hirokazu Anai, Frédéric Chazal, Marc Glisse, Yuichi Ike, Hiroya Inakoshi, Raphaël Tinarrage, and Yuhei Umeda. DTM-based filtrations. In *Topological Data Analysis*, pages 33–66. Springer, 2020.
- [6] Aras Asaad and Sabah Jassim. Topological data analysis for image tampering detection. In *International Workshop on Digital Watermarking*, pages 136–146. Springer, 2017.
- [7] Ulrich Bauer. Ripser: efficient computation of Vietoris-Rips persistence barcodes. *Journal of Applied and Computational Topology*, 2021.
- [8] Paul Bendich, James S Marron, Ezra Miller, Alex Pieloch, and Sean Skwerer. Persistent homology analysis of brain artery trees. *Annals of Applied Statistics*, 10(1):198, 2016.
- [9] Piotr Berman, Meiram Murzabulatov, and Sofya Raskhodnikova. Testing convexity of figures under the uniform distribution. *Random Structures & Algorithms*, 54(3):413–443, 2019.
- [10] Eric Berry, Yen-Chi Chen, Jessi Cisewski-Kehe, and Brittany Terese Fasy. Functional summaries of persistence diagrams. *arXiv preprint arXiv:1804.01618*, 2018.
- [11] Omer Bobrowski and Sayan Mukherjee. The topology of probability distributions on manifolds. *Probability Theory and Related Fields*, 161(3):651–686, 2015.
- [12] Jean-Daniel Boissonnat, Frédéric Chazal, and Mariette Yvinec. *Geometric and Topological Inference*, volume 57. Cambridge University Press, 2018.
- [13] Doug M Boyer, Jesus Puente, Justin T Gladman, Chris Glynn, Sayan Mukherjee, Gabriel S Yapuncich, and Ingrid Daubechies. A new fully automated approach for aligning and comparing shapes. *The Anatomical Record*, 298(1):249–276, 2015.
- [14] Rickard Brüel-Gabrielsson, Bradley J Nelson, Anjan Dwaraknath, Primoz Skraba, Leonidas J Guibas, and Gunnar Carlsson. A topology layer for machine learning. *arXiv preprint arXiv:1905.12200*, 2019.
- [15] Peter Bubenik. Statistical topological data analysis using persistence landscapes. *The Journal of Machine Learning Research*, 16(1):77–102, 2015.

- [16] Peter Bubenik and Paweł Dłotko. A persistence landscapes toolbox for topological statistics. *Journal of Symbolic Computation*, 78:91–114, 2017.
- [17] Peter Bubenik, Michael Hull, Dhruv Patel, and Benjamin Whittle. Persistent homology detects curvature. *Inverse Problems*, 36(2):025008, 2020.
- [18] Zixuan Cang, Lin Mu, and Guo-Wei Wei. Representability of algebraic topology for biomolecules in machine learning based scoring and virtual screening. *PLoS computational biology*, 14(1):e1005929, 2018.
- [19] Zixuan Cang and Guo-Wei Wei. TopologyNet: Topology based deep convolutional and multi-task neural networks for biomolecular property predictions. *PLoS computational biology*, 13(7):e1005690, 2017.
- [20] Gunnar Carlsson. Topological pattern recognition for point cloud data. *Acta Numerica*, 23:289–368, 2014.
- [21] Mathieu Carrière, Frédéric Chazal, Yuichi Ike, Théo Lacombe, Martin Royer, and Yuhei Umeda. PersLay: A neural network layer for persistence diagrams and new graph topological signatures. In *International Conference on Artificial Intelligence and Statistics*, pages 2786–2796. PMLR, 2020.
- [22] Mathieu Carrière, Steve Y Oudot, and Maks Ovsjanikov. Stable topological signatures for points on 3D shapes. In *Computer Graphics Forum*, volume 34, pages 1–12. Wiley Online Library, 2015.
- [23] Frédéric Cazals and Marc Pouget. Estimating differential quantities using polynomial fitting of osculating jets. *Computer Aided Geometric Design*, 22(2):121–146, 2005.
- [24] Frédéric Chazal and David Cohen-Steiner. Geometric inference, 2013.
- [25] Frédéric Chazal, David Cohen-Steiner, André Lieutier, and Boris Thibert. Stability of curvature measures. In *Computer Graphics Forum*, volume 28, pages 1485–1496. Wiley Online Library, 2009.
- [26] Frédéric Chazal, David Cohen-Steiner, and Quentin Mérigot. Geometric inference for probability measures. *Foundations of Computational Mathematics*, 11(6):733–751, 2011.
- [27] Frédéric Chazal, Brittany Fasy, Fabrizio Lecci, Bertrand Michel, Alessandro Rinaldo, Alessandro Rinaldo, and Larry Wasserman. Robust topological inference: Distance to a measure and kernel distance. *The Journal of Machine Learning Research*, 18(1):5845–5884, 2017.
- [28] Frédéric Chazal, Brittany Terese Fasy, Fabrizio Lecci, Alessandro Rinaldo, Aarti Singh, and Larry Wasserman. On the bootstrap for persistence diagrams and landscapes. *arXiv preprint arXiv:1311.0376*, 2013.
- [29] Frédéric Chazal, Leonidas J Guibas, Steve Y Oudot, and Primoz Skraba. Scalar field analysis over point cloud data. *Discrete & Computational Geometry*, 46(4):743–775, 2011.
- [30] Frédéric Chazal and Steve Yann Oudot. Towards persistence-based reconstruction in Euclidean spaces. In *Proceedings of the twenty-fourth annual symposium on Computational geometry*, pages 232–241, 2008.
- [31] Chao Chen, Xiuyan Ni, Qinxun Bai, and Yusu Wang. A topological regularizer for classifiers via persistent homology. In *The 22nd International Conference on Artificial Intelligence and Statistics*, pages 2573–2582. PMLR, 2019.
- [32] Harish Chintakunta, Thanos Gentimis, Rocio Gonzalez-Diaz, Maria-Jose Jimenez, and Hamid Krim. An entropy-based persistence barcode. *Pattern Recognition*, 48(2):391–401, 2015.
- [33] James Clough, Nicholas Byrne, Ilkay Oksuz, Veronika A Zimmer, Julia A Schnabel, and Andrew King. A topological loss function for deep-learning based image segmentation using persistent homology. *IEEE Transactions on Pattern Analysis and Machine Intelligence*, 2020.
- [34] James R Clough, Ilkay Oksuz, Nicholas Byrne, Julia A Schnabel, and Andrew P King. Explicit topological priors for deep-learning based image segmentation using persistent homology. In *International Conference on Information Processing in Medical Imaging*, pages 16–28. Springer, 2019.
- [35] David Cohen-Steiner, Herbert Edelsbrunner, and John Harer. Stability of persistence diagrams. *Discrete & Computational Geometry*, 37(1):103–120, 2007.

- [36] Anne Collins, Afra Zomorodian, Gunnar Carlsson, and Leonidas J Guibas. A barcode shape descriptor for curve point cloud data. *Computers & Graphics*, 28(6):881–894, 2004.
- [37] Loïc Crombez, Guilherme D da Fonseca, and Yan Gérard. Efficient algorithms to test digital convexity. In *International Conference on Discrete Geometry for Computer Imagery*, pages 409–419. Springer, 2019.
- [38] Justin Curry, Sayan Mukherjee, and Katharine Turner. How many directions determine a shape and other sufficiency results for two topological transforms. *arXiv preprint arXiv:1805.09782*, 2018.
- [39] Thibault de Surrél, Felix Hensel, Mathieu Carrière, Théo Lacombe, Yuichi Ike, Hiroaki Kurihara, Marc Glisse, and Frédéric Chazal. RipsNet: a general architecture for fast and robust estimation of the persistent homology of point clouds. *arXiv preprint arXiv:2202.01725*, 2022.
- [40] Herbert Edelsbrunner and John Harer. *Computational topology: An introduction*. American Mathematical Society, 2010.
- [41] Herbert Edelsbrunner, David Kirkpatrick, and Raimund Seidel. On the shape of a set of points in the plane. *IEEE Transactions on information theory*, 29(4):551–559, 1983.
- [42] Herbert Edelsbrunner, David Letscher, and Afra Zomorodian. Topological persistence and simplification. In *Proceedings 41st Annual Symposium on Foundations of Computer Science*, pages 454–463. IEEE, 2000.
- [43] Herbert Edelsbrunner and Ernst P Mücke. Three-dimensional alpha shapes. *ACM Transactions on Graphics (TOG)*, 13(1):43–72, 1994.
- [44] Adélie Garin and Guillaume Tauzin. A topological “reading” lesson: Classification of MNIST using TDA. In *2019 18th IEEE International Conference On Machine Learning And Applications (ICMLA)*, pages 1551–1556. IEEE, 2019.
- [45] Robert Ghrist, Rachel Levanger, and Huy Mai. Persistent homology and Euler integral transforms. *Journal of Applied and Computational Topology*, 2(1):55–60, 2018.
- [46] Noah Giansiracusa, Robert Giansiracusa, and Chul Moon. Persistent homology machine learning for fingerprint classification. *arXiv preprint arXiv:1711.09158*, 2017.
- [47] Barbara Giunti. *TDA-Applications*. zotero database, 2020.
- [48] Paul Guerrero, Yanir Kleiman, Maks Ovsjanikov, and Niloy J Mitra. PCPNET learning local shape properties from raw point clouds. In *Computer Graphics Forum*, volume 37, pages 75–85. Wiley Online Library, 2018.
- [49] Tong He, Haibin Huang, Li Yi, Yuqian Zhou, Chihao Wu, Jue Wang, and Stefano Soatto. GeoNet: Deep geodesic networks for point cloud analysis. In *Proceedings of the IEEE/CVF Conference on Computer Vision and Pattern Recognition*, pages 6888–6897, 2019.
- [50] Christoph Hofer, Roland Kwitt, Marc Niethammer, and Andreas Uhl. Deep learning with topological signatures. *arXiv preprint arXiv:1707.04041*, 2017.
- [51] Umar Islambekov, Monisha Yuvaraj, and Yulia R Gel. Harnessing the power of topological data analysis to detect change points in time series. *arXiv preprint arXiv:1910.12939*, 2019.
- [52] Maria-Jose Jimenez, Belen Medrano, David Monaghan, and Noel E O’Connor. Designing a topological algorithm for 3D activity recognition. In *International Workshop on Computational Topology in Image Context*, pages 193–203. Springer, 2016.
- [53] Tomasz Kaczynski, Konstantin Mischaikow, and Marian Mrozek. *Computational homology*, volume 157. Springer Science & Business Media, 2004.
- [54] Jules Raymond Kala, Serestina Viriri, Deshendran Moodley, and Jules Raymond Tapamo. Leaf classification using convexity measure of polygons. In *International Conference on Image and Signal Processing*, pages 51–60. Springer, 2016.
- [55] Sara Kališnik. Tropical coordinates on the space of persistence barcodes. *Foundations of Computational Mathematics*, 19(1):101–129, 2019.
- [56] Jisu Kim, Jaehyeok Shin, Frédéric Chazal, Alessandro Rinaldo, and Larry Wasserman. Homotopy reconstruction via the Čech complex and the Vietoris-Rips complex. *arXiv preprint arXiv:1903.06955*, 2019.

- [57] Ron Kimmel and Xue-Cheng Tai. *Processing, Analyzing and Learning of Images, Shapes, and Forms: Part 2*. Elsevier, 2019.
- [58] Javier Lamar-León, Edel B Garcia-Reyes, and Rocio Gonzalez-Diaz. Human gait identification using persistent homology. In *Iberoamerican Congress on Pattern Recognition*, pages 244–251. Springer, 2012.
- [59] Longin Jan Latecki, Rolf Lakamper, and T Eckhardt. Shape descriptors for non-rigid shapes with a single closed contour. In *Proceedings IEEE Conference on Computer Vision and Pattern Recognition. CVPR 2000 (Cat. No. PR00662)*, volume 1, pages 424–429. IEEE, 2000.
- [60] Hoanh Le. Geometric invariance of PointNet. *Science and Engineering*, 2021.
- [61] Yongjin Lee, Senja D Barthel, Paweł Dłotko, S Mohamad Moosavi, Kathryn Hess, and Berend Smit. Quantifying similarity of pore-geometry in nanoporous materials. *Nature Communications*, 8(1):1–8, 2017.
- [62] Javier Lamar Leon, Raúl Alonso, Edel Garcia Reyes, and Rocio Gonzalez Diaz. Topological features for monitoring human activities at distance. In *International Workshop on Activity Monitoring by Multiple Distributed Sensing*, pages 40–51. Springer, 2014.
- [63] Mao Li, Hong An, Ruthie Angelovici, Clement Bagaza, Albert Batushansky, Lynn Clark, Viktoriya Coneva, Michael J Donoghue, Erika Edwards, Diego Fajardo, et al. Topological data analysis as a morphometric method: using persistent homology to demarcate a leaf morphospace. *Frontiers in Plant Science*, 9:553, 2018.
- [64] Mao Li, Margaret H Frank, Viktoriya Coneva, Washington Mio, Daniel H Chitwood, and Christopher N Topp. The persistent homology mathematical framework provides enhanced genotype-to-phenotype associations for plant morphology. *Plant Physiology*, 177(4):1382–1395, 2018.
- [65] Kart-Leong Lim and Hamed Kiani Galoogahi. Shape classification using local and global features. In *2010 Fourth Pacific-Rim Symposium on Image and Video Technology*, pages 115–120. IEEE, 2010.
- [66] Joseph SB Mitchell, David M Mount, and Christos H Papadimitriou. The discrete geodesic problem. *SIAM Journal on Computing*, 16(4):647–668, 1987.
- [67] Guido Montúfar, Nina Otter, and Yuguang Wang. Can neural networks learn persistent homology features? *arXiv preprint arXiv:2011.14688*, 2020.
- [68] Gregory Naitzat, Andrey Zhitnikov, and Lek-Heng Lim. Topology of deep neural networks. *J. Mach. Learn. Res.*, 21(184):1–40, 2020.
- [69] Partha Niyogi, Stephen Smale, and Shmuel Weinberger. Finding the homology of submanifolds with high confidence from random samples. *Discrete & Computational Geometry*, 39(1-3):419–441, 2008.
- [70] Ipppei Obayashi, Yasuaki Hiraoka, and Masao Kimura. Persistence diagrams with linear machine learning models. *Journal of Applied and Computational Topology*, 1(3-4):421–449, 2018.
- [71] Nina Otter. Magnitude meets persistence. Homology theories for filtered simplicial sets. *arXiv preprint arXiv:1807.01540*, 2018. to appear in *Homology, Homotopy and Applications*.
- [72] Nina Otter, Mason A Porter, Ulrike Tillmann, Peter Grindrod, and Heather A Harrington. A roadmap for the computation of persistent homology. *EPJ Data Science*, 6(1):17, 2017.
- [73] Rahul Paul and Stephan Chalup. Estimating Betti numbers using deep learning. In *2019 International Joint Conference on Neural Networks (IJCNN)*, pages 1–7. IEEE, 2019.
- [74] Jose A Perea, Anastasia Deckard, Steve B Haase, and John Harer. Swlpers: Sliding windows and 1-persistence scoring; discovering periodicity in gene expression time series data. *BMC Bioinformatics*, 16(1):257, 2015.
- [75] Giovanni Petri, Martina Scolamiero, Irene Donato, and Francesco Vaccarino. Topological strata of weighted complex networks. *PLOS ONE*, 8(6):e66506, 2013.
- [76] James R Pomerantz. Wholes, holes, and basic features in vision. *Trends in Cognitive Sciences*, 7(11):471–473, 2003.

- [77] Rolandos Alexandros Potamias, Alexandros Neofytou, Kyriaki Margarita Bintsi, and Stefanos Zafeiriou. GraphWalks: Efficient shape agnostic geodesic shortest path estimation. In *Proceedings of the IEEE/CVF Conference on Computer Vision and Pattern Recognition*, pages 2968–2977, 2022.
- [78] Charles R Qi, Hao Su, Kaichun Mo, and Leonidas J Guibas. PointNet: Deep learning on point sets for 3D classification and segmentation. <https://github.com/charlesq34/pointnet>. Accessed: 2022-02-01.
- [79] Charles R Qi, Hao Su, Kaichun Mo, and Leonidas J Guibas. PointNet: Deep learning on point sets for 3D classification and segmentation. In *Proceedings of the IEEE Conference on Computer Vision and Pattern Recognition*, pages 652–660, 2017.
- [80] Archit Rathore, Sourabh Palande, Jeffrey S Anderson, Brandon A Zielinski, P Thomas Fletcher, and Bei Wang. Autism classification using topological features and deep learning: a cautionary tale. In *International Conference on Medical Image Computing and Computer-Assisted Intervention*, pages 736–744. Springer, 2019.
- [81] Vanessa Robins. Computational topology for point data: Betti numbers of  $\alpha$ -shapes. In *Morphology of Condensed Matter*, pages 261–274. Springer, 2002.
- [82] Christian Ronse. A bibliography on digital and computational convexity (1961–1988). *IEEE Transactions on Pattern Analysis and Machine Intelligence*, 11(2):181–190, 1989.
- [83] Martin Royer, Frédéric Chazal, Clément Levrard, Yuichi Ike, and Yuhei Umeda. ATOL: Measure vectorisation for automatic topologically-oriented learning. *arXiv preprint arXiv:1909.13472*, 2019.
- [84] Matteo Rucco, Filippo Castiglione, Emanuela Merelli, and Marco Pettini. Characterisation of the idiotypic immune network through persistent entropy. In *Proceedings of ECCS 2014*, pages 117–128. Springer, 2016.
- [85] Gunnar Schmidtman, Ben J Jennings, and Frederick AA Kingdom. Shape recognition: convexities, concavities and things in between. *Scientific Reports*, 5(1):1–11, 2015.
- [86] Benjamin Schweinhart. Fractal dimension and the persistent homology of random geometric complexes. *Advances in Mathematics*, 372:107291, 2020.
- [87] D.R. Sheehy. Linear-size approximations to the vietoris–rips filtration. *Discrete & Computational Geometry*, page 778–796, 2013.
- [88] Thomas Sikora. The MPEG-7 visual standard for content description-an overview. *IEEE Transactions on Circuits and Systems for Video Technology*, 11(6):696–702, 2001.
- [89] Nikhil Singh, Heather D Couture, JS Marron, Charles Perou, and Marc Niethammer. Topological descriptors of histology images. In *International Workshop on Machine Learning in Medical Imaging*, pages 231–239. Springer, 2014.
- [90] Primož Skraba and Katharine Turner. Wasserstein stability for persistence diagrams. *arXiv preprint arXiv:2006.16824*, 2020.
- [91] Bernadette J Stolz, Heather A Harrington, and Mason A Porter. Persistent homology of time-dependent functional networks constructed from coupled time series. *Chaos: An Interdisciplinary Journal of Nonlinear Science*, 27(4):047410, 2017.
- [92] The GUDHI Project. *GUDHI User and Reference Manual*. GUDHI Editorial Board, 3.3.0 edition, 2020.
- [93] The RIVET Developers. Rivet, 2020.
- [94] Christopher Tralie, Nathaniel Saul, and Rann Bar-On. Ripser.py: A lean persistent homology library for python. *The Journal of Open Source Software*, 3(29):925, Sep 2018.
- [95] Renata Turkeš, Jannes Nys, Tim Verdonck, and Steven Latré. Noise robustness of persistent homology on greyscale images, across filtrations and signatures. *PLOS ONE*, 16(9):e0257215, 2021.
- [96] Katharine Turner, Sayan Mukherjee, and Doug M Boyer. Persistent homology transform for modeling shapes and surfaces. *Information and Inference: A Journal of the IMA*, 3(4):310–344, 2014.
- [97] Katharine Turner and Gard Spreemann. Same but different: Distance correlations between topological summaries. In *Topological Data Analysis*, pages 459–490. Springer, 2020.

- [98] Yuhei Umeda. Time series classification via topological data analysis. *Information and Media Technologies*, 12:228–239, 2017.
- [99] Oliver Vipond. Multiparameter persistence landscapes. *J. Mach. Learn. Res.*, 21(61):1–38, 2020.
- [100] Pauli Virtanen, Ralf Gommers, Travis E Oliphant, Matt Haberland, Tyler Reddy, David Cournapeau, Evgeni Burovski, Pearu Peterson, Warren Weckesser, Jonathan Bright, et al. SciPy 1.0: fundamental algorithms for scientific computing in Python. *Nature methods*, 17(3):261–272, 2020.
- [101] Menglun Wang, Zixuan Cang, and Guo-Wei Wei. A topology-based network tree for the prediction of protein–protein binding affinity changes following mutation. *Nature Machine Intelligence*, 2(2):116–123, 2020.
- [102] Yan Wang, Yining Zhao, Shihui Ying, Shaoyi Du, and Yue Gao. Rotation-invariant point cloud representation for 3-D model recognition. *IEEE Transactions on Cybernetics*, 2022.
- [103] Eugene P Wigner. The unreasonable effectiveness of mathematics in the natural sciences. *Communications on Pure and Applied Mathematics*, 13:1–14, 1960.
- [104] Chi-Chong Wong and Chi-Man Vong. Persistent homology based graph convolution network for fine-grained 3D shape segmentation. In *Proceedings of the IEEE/CVF International Conference on Computer Vision*, pages 7098–7107, 2021.
- [105] Stephen Gang Wu, Forrest Sheng Bao, Eric You Xu, Yu-Xuan Wang, Yi-Fan Chang, and Qiao-Liang Xiang. A leaf recognition algorithm for plant classification using probabilistic neural network. In *2007 IEEE International Symposium on Signal Processing and Information Technology*, pages 11–16. IEEE, 2007.
- [106] Chenxi Xiao and Juan Wachs. Triangle-Net: Towards robustness in point cloud learning. In *Proceedings of the IEEE/CVF Winter Conference on Applications of Computer Vision*, pages 826–835, 2021.
- [107] Junming Zhang, Ming-Yuan Yu, Ram Vasudevan, and Matthew Johnson-Roberson. Learning rotation-invariant representations of point clouds using aligned edge convolutional neural networks. In *2020 International Conference on 3D Vision (3DV)*, pages 200–209. IEEE, 2020.
- [108] Zhiyuan Zhang, Binh-Son Hua, David W Rosen, and Sai-Kit Yeung. Rotation invariant convolutions for 3D point clouds deep learning. In *2019 International Conference on 3D Vision (3DV)*, pages 204–213. IEEE, 2019.
- [109] Ziwei Zhang, Xin Wang, Zeyang Zhang, Peng Cui, and Wenwu Zhu. Revisiting transformation invariant geometric deep learning: Are initial representations all you need? *arXiv preprint arXiv:2112.12345*, 2021.
- [110] Chen Zhao, Jiaqi Yang, Xin Xiong, Angfan Zhu, Zhiguo Cao, and Xin Li. Rotation invariant point cloud analysis: Where local geometry meets global topology. *Pattern Recognition*, page 108626, 2022.
- [111] Qi Zhao, Ze Ye, Chao Chen, and Yusu Wang. Persistence enhanced graph neural network. In *International Conference on Artificial Intelligence and Statistics*, pages 2896–2906. PMLR, 2020.
- [112] Zhen Zhou, Yongzhen Huang, Liang Wang, and Tieniu Tan. Exploring generalized shape analysis by topological representations. *Pattern Recognition Letters*, 87:177–185, 2017.
- [113] Afra Zomorodian and Gunnar Carlsson. Computing persistent homology. *Discrete & Computational Geometry*, 33(2):249–274, 2005.
- [114] Jovisa Zunic and Paul L Rosin. A new convexity measure for polygons. *IEEE Transactions on Pattern Analysis and Machine Intelligence*, 26(7):923–934, 2004.

## Appendix

The appendix is organized into the following sections.

- Appendix A Theoretical results
- Appendix B: Experimental details; pipelines, training and hyperparameter tuning

- Appendix C: Additional experimental details for number of holes
- Appendix D: Additional experimental details for curvature
- Appendix E: Additional experimental details for convexity
- Appendix F: Guidelines for persistent homology in applications; long and short persistence intervals
- Appendix G: Persistent homology detects convexity in FLAVIA dataset

## A Theoretical results

In this section, we provide the proof of our Theorem 1 that guarantees that PH can be used to detect convexity. We then formulate Theorem 6 and Theorem 7 from the literature, that summarise known theoretical guarantees that PH can detect the number of holes and curvature. At the end of the section, we also discuss some known results about the theoretical computational complexity of PH.

### A.1 Convexity

In our pipeline for the detection of convexity we consider filtrations associated to different height functions, defined as follows.

**Definition 2.** Given a line  $\ell \subset \mathbb{R}^2$ , we define the **height function with respect to  $\ell$**  as follows:

$$h_\ell: \mathbb{R}^2 \rightarrow \mathbb{R} : p \mapsto \text{dist}(p, \ell)$$

where  $\text{dist}(p, \ell)$  is the distance of the point  $p$  from the line  $\ell$ .

Given  $X \subset \mathbb{R}^2$  and a line  $\ell$  we are interested in studying the subsets of  $X$  consisting of points at a specific distance from the line. We define

$$X_{h_\ell, r} = \{x \in X \mid \text{dist}(x, \ell) \leq r\}.$$

We call  $\{X_{h_\ell, r}\}_{r \in \mathbb{R}_{\geq 0}}$  the **height filtration with respect to  $\ell$** , or alternatively, the **height filtration in direction orthogonal to  $\ell$** .

As an example, we consider Figure 7(a): in cyan we depict the points of the annulus-like shape in  $\mathbb{R}^2$  that are at a certain distance from a line  $\ell$ . In our pipeline, depicted in Figure 18, we consider height filtrations for 9 different lines: for instance, the line passing through the center of the image and parallel to the horizontal boundaries of the image. In this case, the filtration is built by considering all points above and below this line, at a certain distance from it. In the pipeline we indicate the direction of the filtration with two arrows departing from the center of the image and pointing upwards and downwards, respectively.

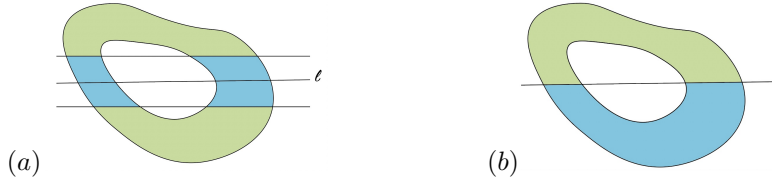


Figure 7: (a) In cyan we illustrate the subspace given by points at a certain distance from a line  $\ell$ . (b) In cyan an example of sublevel set used to define the Persistent Homology Transform.

**Remark 3** (Relationship with the Persistent Homology Transform). There is a lot of work done on studying PH of filtrations associated to height filtrations, see, e.g., [96, 38, 45] in which height filtrations are used to define the Persistent Homology Transform (PHT), a topological summary that has been shown to be a sufficient statistics for probability densities on the space of triangulable subspaces of  $\mathbb{R}^2$  and  $\mathbb{R}^3$ , respectively [96]. The filtrations used in the definition of PHT differ from ours: for a triangulable subspace  $X$  of  $\mathbb{R}^2$  or  $\mathbb{R}^3$ , and a unit vector  $u$ , one considers the filtration given by  $X_{u, r} = \{x \in X \mid x \cdot u \leq r\}$ . We illustrate an example of such a sublevel set in Figure 7(b). The PHT then is given by considering all unit vectors, and computing the persistent homology in degree 0 for the height filtration in each direction.



For practical purposes it would not be feasible to have to consider all unit vectors in the PHT. Luckily, there are known results on the sufficient number of directions [38]. In computational experiments in [96] on the MPEG-7 silhouette database of simulated shapes in  $\mathbb{R}^2$  [88, 59] and point clouds in  $\mathbb{R}^3$  obtained from micro-CT scans of heel bones [13], the PHT is approximated by looking respectively at 64 evenly spaced directions and 162 directions constructed by subdividing an icosahedron. Furthermore, 0- and/or 1-dimensional PH with respect to the height and/or related radial filtration has also been used as a 3-dimensional shape descriptor in [22], for analysis of brain artery trees [8], classification of MNIST images of handwritten digits [44].

The theoretical results related to the Persistent Homology Transform focus on a complete description of shapes, whereas here we are interested in investigating to what extent PH can detect convexity and concavity. For this purpose, and in particular, to be able to detect concavity, we need to consider the different definition of height filtration, given in Definition 2, see also Remark 5.

**Theorem 4.** *Let  $X \subset \mathbb{R}^2$  be triangulable. Let  $\ell$  be any line in  $\mathbb{R}^2$ , and denote by  $h_\ell$  the height function with respect to  $\ell$ . For any  $r \in \mathbb{R}_{\geq 0}$ , denote by  $X_{h_\ell, r}$  the subset of points at distance at most  $r$  from  $\ell$ . Then  $X$  is convex if and only if the persistence diagram in degree 0 of the filtered space  $\{X_{h_\ell, r}\}_{r \in \mathbb{R}_{\geq 0}}$  contains exactly one interval.*

*Proof.* Suppose that  $X$  is convex. By definition, we have that for all  $p_1, p_2 \in X$  the straight-line segment through  $p_1$  and  $p_2$  is contained in  $X$ . A fortiori we have that  $X$  is path connected. Let  $\ell$  be any line in  $\mathbb{R}^2$  and  $r \in \mathbb{R}$  arbitrary. Then we have that  $X_{h_\ell, r}$  is path-connected. Indeed, suppose that  $p_1, p_2 \in X$  are such that  $h_\ell(p_i) \leq r$  for  $i = 1, 2$ . The straight-line segment between  $p_1$  and  $p_2$  is fully contained in  $X$ , and we have that all the points  $q$  on this line segment have height contained between  $h_\ell(p_1)$  and  $h_\ell(p_2)$ , and thus the straight-line segment between  $p_1$  and  $p_2$  is contained in  $X_{h_\ell, r}$ . As a consequence, we have that for any line  $\ell$ , the persistence diagram in degree 0 of  $\{X_{h_\ell, r}\}_{r \in \mathbb{R}}$  contains a single interval.

Next, assume that  $X$  is concave. By definition, there exist  $p_1, p_2 \in X$  and  $q \in \mathbb{R}^2$  such that  $q$  lies on the straight-line segment between  $p_1$  and  $p_2$  and  $q \notin X$ . We have that  $\mathbb{R}^2 \setminus X$  is open, and therefore there exists  $\epsilon > 0$  such that  $B_\epsilon(q) \subset \mathbb{R}^2 \setminus X$ . Let  $\ell$  be the line through  $p_1$  and  $p_2$ . Then  $X_{h_\ell, r}$  is not path-connected for any  $r \leq \epsilon$ : indeed, suppose that we can connect  $p_1$  and  $p_2$  through a path in  $X_{h_\ell, r}$ . Then such a path would have to intersect the line passing through  $q$  and orthogonal to  $\ell$ . By construction this point of intersection would need to be in the ball  $B_\epsilon(q) \setminus X$ , thus leading to a contradiction.

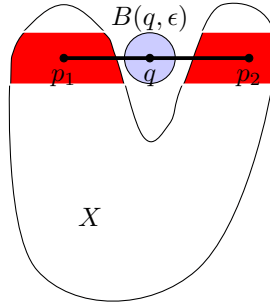


Figure 8: For concave shapes, there exists a height filtration direction so that the resulting 0-dimensional PD sees multiple path-connected components (in red).

□

**Remark 5.** We note that for PH to be able to detect concavity by only computing 0-dimensional PH, we cannot consider height filtrations as the ones used for the Persistent Homology Transform: indeed, consider the annulus-like subset  $X$  of  $\mathbb{R}^2$  illustrated in Figure 7. Then there is no unit vector  $u$  for which the sublevel set  $X_{u, r} = \{x \in X \mid x \cdot u \leq r\}$  contains more than one path component. In such a case, one would need to also compute 1-dimensional PH to be able to detect that the subset is concave. More precisely, one can formulate a statement analogous to the one in Theorem 1 for these different types of height filtrations: one would have that if a triangulable subset of  $\mathbb{R}^2$  is convex, then the persistence diagram in degree 0 of the filtered space  $\{X_{u, r}\}_r$  contains exactly one interval.

Conversely, if  $X$  is concave, then either the persistence diagram in degree 0 of the filtered space  $\{X_{u,r}\}_{r \in \mathbb{R}_{\geq 0}}$  contains more than one interval, or it contains one interval, but the persistence diagram in degree 1 is non-empty.

## A.2 Number of holes

In our pipeline to detect the number of holes, we use the alpha complex, for which several theoretical guarantees have been proven.

The Nerve Lemma (see, e.g., [40]) guarantees that the alpha complex of a set of points has the same homology-type as the space obtained by taking unions of balls of a certain radius centered around the points. Whether this union of balls has the same homology-type as the space from which the points are sampled depends on properties of the sample. If the sample is dense enough, then it has been shown that, for a suitable value of the scaling parameter, the alpha complex has the same number of holes as the original space, for instance under the assumption on the space being a smooth manifold [69]. For ease of reference, we reproduce here the result from [69].

**Theorem 6** (Number of holes). *Let  $S$  be a compact smooth manifold, and  $X$  a set of points sampled uniformly at random from  $S$ . Then there exists  $r \in \mathbb{R}$  such that the homology of the alpha simplicial complex  $\alpha(X, r)$  is isomorphic to the singular homology of the underlying manifold  $X$ .*

*Proof.* [69, Theorem 3.1] implies that there exists  $r \in \mathbb{R}$  such that the singular homology of the  $\cup_{x \in X} B(x, r)$  is isomorphic to the singular homology of  $S$ . By the Nerve Lemma we then know that the simplicial homology of the alpha complex  $\alpha(X, r)$  is isomorphic to the singular homology of  $\cup_{x \in X} B(x, r)$ .  $\square$

The alpha complex is known to approximate the Vietoris–Rips complex, in the sense that the respective persistence modules are interleaved, see, e.g. [40].

## A.3 Curvature

Here we reproduce the theoretical guarantee provided in [17].

**Theorem 7** (Curvature). *Let  $S$  be a manifold with constant curvature  $K$ , and  $D_K$  be a unit disk on  $S$ . Let further  $X$  be a point cloud sampled from  $X$ , according to the probability measure proportional to the surface area measure. Then, PH of  $X$  recovers  $K$ .*

*Proof.* Given  $K$ , [17, Theorem 14] establishes an analytic expression for the persistence ( $p = d/b$ ) of triangles to the curvature  $K$  of the underlying manifold. This function is continuous and increasing, so that persistence recovers curvature.  $\square$

## A.4 Computational complexity

In this section we discuss how our pipelines are affected by the dimension  $d$  of the embedding space and the size  $n$  of the point cloud.

There exist several efficient algorithms for the computation of PH, many coming with heuristic guarantees on speed-ups for the computation (see survey [72] for an overview). For the purposes of this discussion, we will focus on the standard algorithm, which has a computational complexity which is cubical in the number of simplices contained in the filtered simplicial complex. Thus, to better understand how our pipelines generalise to higher-dimensional point clouds, in the following we explain how the sizes of the different types of simplicial complexes that we consider are affected by the dimension and size of the point cloud.

For the detection of holes we compute PH with the alpha complex. In the worst case, the size of the alpha complex is  $\mathcal{O}(n^{\lceil d/2 \rceil})$ . On the other hand, the size of the Vietoris–Rips complex — we recall that this is approximated by the alpha complex — is  $\mathcal{O}(n^{k+2})$ , where  $k$  is the maximum PH degree that we are interested in computing. Thus, in our case, we have that  $k = 1$  and the size is  $\mathcal{O}(n^3)$ .

If we were interested in extending our methods to point-clouds in higher dimensional embedding spaces, the Vietoris–Rips complex would be better suited than the alpha complex for the experiments.

The pipeline for the computation of PH with respect to the Vietoris–Rips filtration takes as input the distance matrix of the points, which can be computed in  $\mathcal{O}(d)$ , while the remaining pipeline is independent of the dimension of the embedding space. Therefore, given the distance matrix, the PH pipeline for the detection of holes and curvature can be easily extended to point clouds in higher dimensional spaces, *provided* one uses efficient algorithms for the computation of PH with the Vietoris–Rips complex, for instance, by using sparsification techniques [87]. On the other hand, the computational complexity of the alpha complex becomes prohibitive in high-dimensional spaces. In practice, the alpha complex is used for 2- and 3-dimensional spaces. A summary of computational complexity of several algorithms for the computation of PH is provided in [72], see in particular Table 1 therein for a summary concerning different types of simplicial complexes, and related references.

Detecting convexity poses additional challenges. Testing convexity is fundamentally a hard problem in high dimensions, related to the hardness of computing convex hulls in high dimensions, and unfortunately we cannot hope for free lunch. In our PH convexity detection pipeline, unlike for the detection of the number of holes or curvature, we calculate PH across multiple height-filtration directions, whose number also grows with the dimension since sufficiently many filtrations need to be considered (and the same would be the case - we would have to consider multiple height directions, if we considered simplicial instead of cubical complexes, see Figure 19). This could be circumvented by considering (quasi-)random directions.

Next to an increased number of filtration directions, additional issues arise, but there are several possible ways to generalize our pipeline to higher dimensions. Consider an example of a concave surface in  $\mathbb{R}^3$  that resembles a ball with a dent on the north pole, i.e., a crater. For arbitrarily many height filtration directions, this concavity cannot be detected with 0-dimensional PH. For the example surface, an interesting direction would be looking at the surface "from the top", but PH would start by seeing a circle, and then the crater itself - always a single connected component. However, 1-dimensional PH with respect to this direction would capture a hole, implying that the surface is concave. In general, for surfaces in  $\mathbb{R}^d$ , we would consider PH in homology degrees  $0, 1, \dots, d - 1$ . Alternatively, an idea could be to study *computable* invariants for multi-parameter persistence in degree 0, by scanning shapes from multiple directions *simultaneously*. We note that while the theory and computations for multi-parameter persistence are hard, there have been some recent advances, see, e.g., [93]. For the example shape, 0-dimensional PH would capture the two connected components with the bi-filtration that looks at the shape from the top, and also from an orthogonal direction from the center of the shape. This is an interesting avenue for further work.

To conclude, specifying a desired computation budget and number of filtrations in advance (leading to a corresponding accuracy tradeoff), our PH pipeline can be used to obtain fast estimates of convexity. It can also be used to compute a continuous measure of convexity (as we demonstrate on the real-world FLAVIA dataset of leaf images in Appendix G), or convexity at a given resolution, depending on the resolution of the filtration, which in some cases may be more useful than the binary label.

## B Experimental details

### B.1 Reproducibility and computer infrastructure

The data and code developed for this research are made publicly available at <https://github.com/renata-turkes/turkevs2022on>. All our computations were conducted using a 2.7Ghz vCPU core from a DGX-1 + DGX-2 station.

### B.2 Hyperparameter tuning and training procedure for the individual pipelines

In this section, we provide more details about the pipelines that were compared in the computational experiments:

- SVM on persistent homology features (PH),
- simple machine learning (ML) baseline - SVM on distance matrices,
- fully connected neural network (NN) on distance matrices, and
- PointNet (PointNet) on raw point clouds.

For each pipeline, we list the hyperparameters that were tuned. We used `sklearn GridSearchCV` based on cross validation with 3 folds and random splits, and returned the hyperparameter values that resulted in the highest accuracy for classification problems (Section 3 and Section 5), or the lowest mean squared error for regression problems (Section 4). We also list relevant software and licenses.

**PH** The general steps to extract PH features are visualized in Figure 9. To calculate PH in Section 3 and Section 5 we use GUDHI [92], and in Section 4 we use `Ripser` [7, 94], which are persistent homology libraries in Python, available under the MIT (GPL v3) license. For the DTM filtration in Section 3, we choose  $m = 0.03$ , so that  $0.03 \times 1000 = 30$  nearest neighbors are used to calculate the filtration function. To build the filtration in Section 5, we consider a  $20 \times 20$  grid for cubical complexes. Grid search is performed to choose the best persistence signature and classifier or regressor as described below.

- In Section 3 and Section 4, we select between:
  - simple signature of 10 longest lifespans,
  - persistence images with resolution  $10 \times 10$ , bandwidth  $\sigma \in \{0.1, 0.5, 1, 10\}$ , and weight function  $\omega(x, y) \in \{1, y, y^2\}$ , and
  - persistence landscapes with resolution of 100, and considering the longest 1, 10 or all persistence intervals.
- We use SVM (`sklearn SVC` and `SVR` for classification and regression respectively) on the PH signature, with the regularization parameter  $C \in \{0.001, 1, 100\}$ . The latter tunes the trade off between correct classification of training data and maximization of the decision function’s margin.

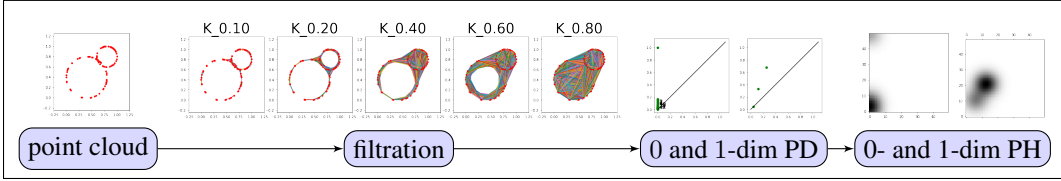


Figure 9: Persistent homology features. To calculate PH for the given point cloud in  $\mathbb{R}^2$ , we first construct a filtration  $K_1 \subseteq K_2 \subseteq \dots K_r \subseteq \dots K_k$  which approximates  $X$  at different scales  $r \in \mathbb{R}$ , where  $K_r$  is the Vietoris-Rips simplicial complex. 0-dimensional PD has one persistent cycle, reflecting the single connected component, and a number of short cycles that correspond to the individual point-cloud points that are connected to other ones early in the filtration. 1-dimensional PD summarizes the two holes, whose birth and death values respectively reflect the sparsity along the hole and the size of the hole, as these are the scales  $r \in \mathbb{R}$  at which the hole appears and when it is filled in within the filtration. PDs are then represented by PIs, which are vector summaries that can be used in statistical learning frameworks, but many other signatures (denoted, in general, with PH) can be used.

**ML** In our experiment, the input for the simple machine learning (ML) pipeline is the matrix of pairwise Euclidean distances between point-cloud points. For a given point cloud  $X = \{\mathbf{x}_1, \dots, \mathbf{x}_N\} \subset \mathbb{R}^d$ , the corresponding distance matrix is the  $N \times N$  matrix  $D \in \mathbb{R}^{N \times N}$  with entries  $D_{ij} = \|\mathbf{x}_i - \mathbf{x}_j\|$ . We take the entries above the diagonal flattened into a vector. Since the dimension of distance matrices scales with the square of the number of points, we work with subsamples of 100 distinct random points from each point cloud. This allowed us to train the SVMs on data sets with 1000 point clouds. Similarly as above, we use cross validation to choose the SVM regularization parameter among  $C \in \{0.001, 1, 100\}$ .

We note that while a distance matrix can be taken as input to a classifier, it depends on the particular and arbitrary labeling of the points in the point cloud and hence it does not account for the label symmetry of point clouds.

**NN** The distance matrices are also fed to the multi-layer perceptrons (MLPs). We consider the following hyperparameters:

- depth in  $\{1, 2, 3, 4, 5\}$  (only for NN deep),
- layer widths in  $\{64, 256, 1024\}$ ,
- learning rate in  $\{0.01, 0.001\}$ ,

that are selected through a grid search, with each parameter setting trained for 2 epochs. We use a softmax activation function, and cross entropy and mean squared error as loss functions for classification (Section 3 and Section 5) and regression (Section 4) problems, respectively.

**PointNet** PointNet [79] is a neural network that takes point clouds as inputs, and is inspired by the invariance of point clouds to permutations and transformations. It incorporates fully-connected MLPs to approximate classification functions, and convolutional layers to capture geometric relationships between features.

In our experiments, we rely on the PointNet model from `keras` [1] under Apache License 2.0. This model implements the architecture from the original PointNet paper [79], which is supplemented with a publicly available code [78], licensed under MIT. We use grid search to tune:

- number of filters in  $\{32, 64\}$ ,
- learning rate in  $\{0.01, 0.001\}$ .

For each of the problems we consider, the model is trained from scratch using the training set described in the corresponding section.

## C Additional experimental details for number of holes

### C.1 Data transformations

To test the noise robustness of the different pipelines, in Section 3 we consider the test data consisting of the original point clouds, or point clouds under different transformations (Figure 2). A detailed description of the data transformations is given in Table 1, and the transformations are visualized on an example point cloud in Figure 10. To define reasonable values for the data transformations, we took inspiration from the affNIST<sup>6</sup> dataset of MNIST images under affine transformations.

Table 1: Data transformations.

Transformation	Definition of transformation
rotation	Clockwise rotation by an angle chosen uniformly from $[-20, 20]$ degrees clockwise.
translation	Translation by random numbers chosen from $[-1, 1]$ for each direction.
stretch	Scale by a factor chosen uniformly from $[0.8, 1.2]$ in the $x$ -direction. The other coordinates remain unchanged, so that the point cloud is stretched. Stretching factor of 0.8 results in shrinking the point cloud by 20%, and the factor of 1.2 makes it 20% larger.
shear	Shear by a factor chosen uniformly from $[-0.2, 0.2]$ . A shearing factor of 1 means that a horizontal line turns into a line at 45 degrees.
Gaussian noise	Random noise drawn from normal distribution $\mathcal{N}(0, \sigma)$ with the standard deviation $\sigma$ uniformly chosen from $[0, 0.1]$ is added to the point cloud.
outliers	A percentage, chosen uniformly from $[0, 0.1]$ , of point cloud points are replaced with points sampled from a uniform distribution within the range of the point cloud.

<sup>6</sup><https://www.cs.toronto.edu/~tijmen/affNIST/>

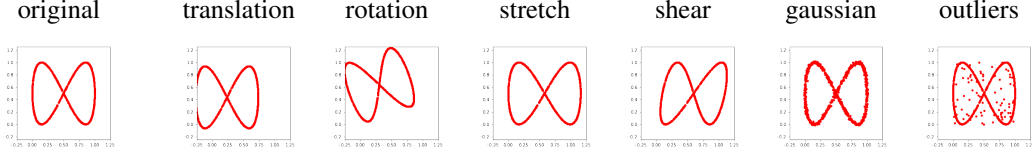


Figure 10: An example point cloud under the considered transformations.

## C.2 Pipeline

Figure 11 visualizes the PH pipeline. To reduce the computation times, we approximate point clouds at each scale with the alpha simplicial complex (discussed in Section 2, and in particular, in Section 2.1). The DTM filtration on the point-cloud points is defined as the average distance from a number of nearest neighbors. Therefore, outliers appear only late in the filtration, so that their influence is smoothed out to a great extent. For the example point cloud in the figure, the 1-dimensional PD consists of four persistence intervals with non-negligible persistence or lifespan (PD points far from diagonal) which correspond to the four big holes, and many short persistence intervals that correspond to holes that are seen at some scales due to noise. This is clearly reflected in the vector of sorted lifespans of the 10 most persisting cycles.

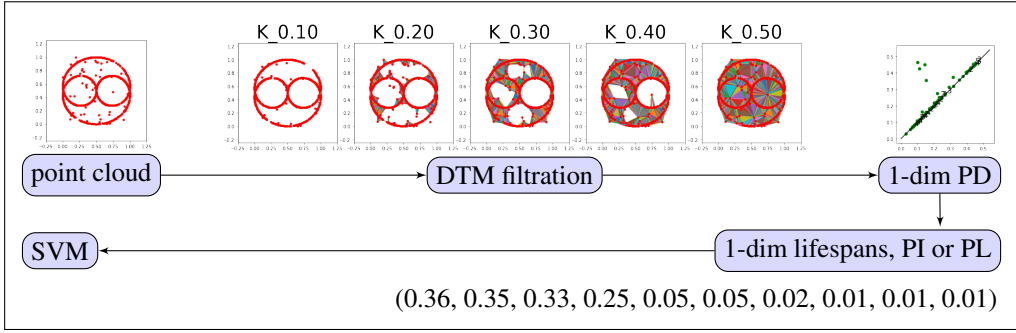


Figure 11: Persistent homology pipeline to detect the number of holes.

## C.3 Training curves

Figure 12 shows the training curves for the NN and PointNet pipelines. The training set performance of MLPs (shallow and deep) continues improving over epochs, but the validation set performance quickly saturates and stops improving after a few epochs. PointNet performs well on this task, already after a short number of training epochs. We do not include training curves for the PH and ML pipelines, as these are based on SVMs.

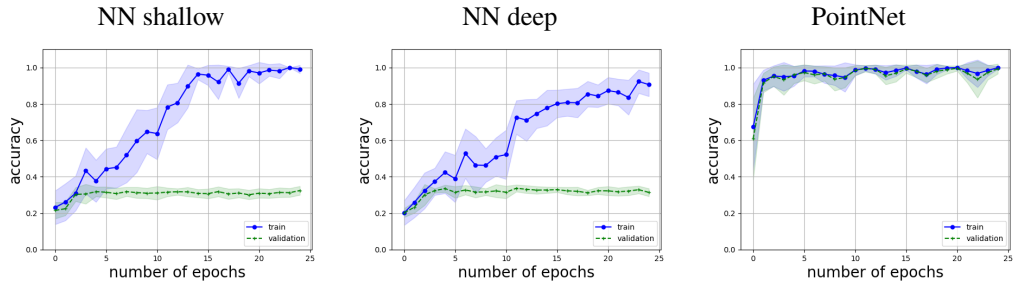


Figure 12: Training curves for the detection of the number of holes.

## C.4 Learning curves

Figure 13 shows the learning curves for every pipeline; i.e., the test accuracy of the trained pipelines depending on the total amount of training data. This serves to evaluate the data efficiency of the different methods. The PH-approaches perform well even for a small number of training point clouds. PointNet also has good performance, although it requires more training data. The other approaches (NN shallow, NN deep, and ML) have poor performance, which does not improve when more training data is available. An explanation for this is that these methods are based on distance matrices and hence cannot directly take advantage of the permutation symmetry of point clouds.

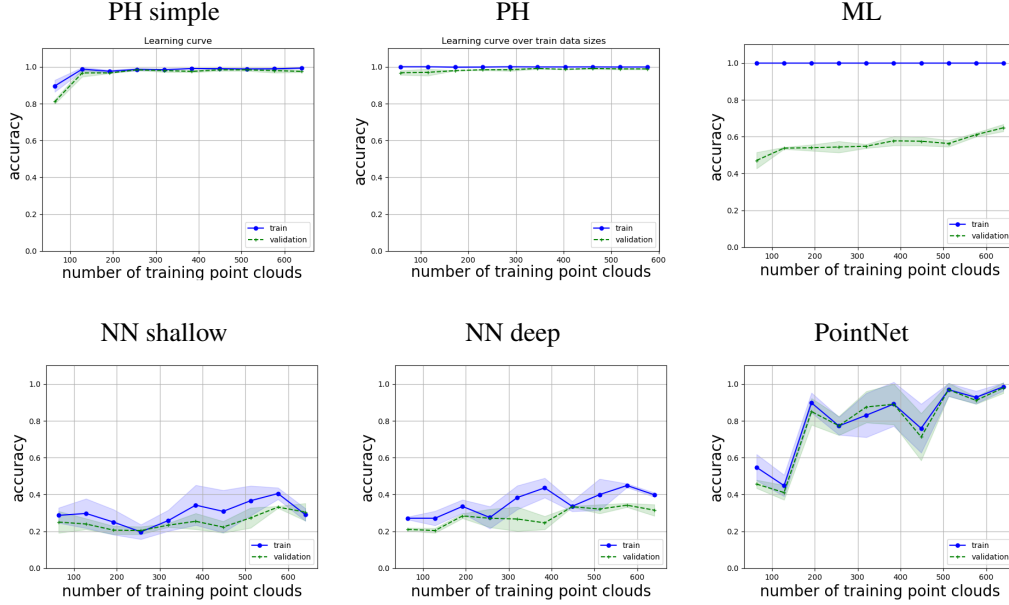


Figure 13: Learning curves for the detection of the number of holes.

## C.5 Computational resources

Figure 14 visualizes the computational efficiency and memory usage. We see that PH pipeline also performs better with respect to these criteria in comparison to the other methods. We note that the difference in the memory usage for data comes from the different types of input that are considered by different pipelines: PDs (lists of persistence intervals) for PH simple and PH,  $100 \times 100$  distance matrices for ML and NNs, and  $1000 \times 3$  point clouds for PointNet (Appendix B.2).

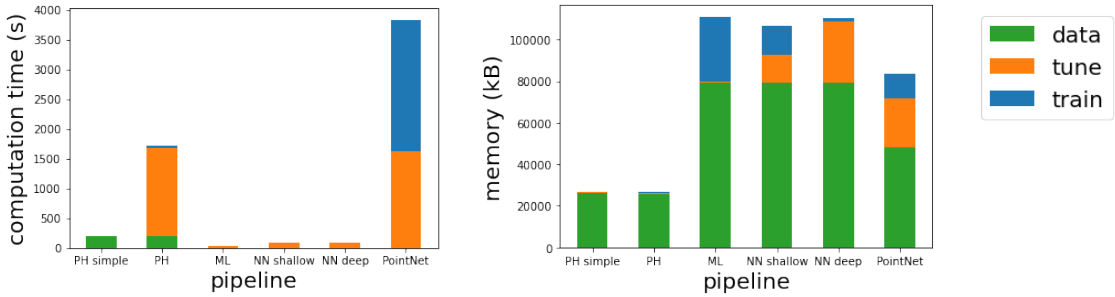


Figure 14: Computational resources for the detection of the number of holes.

## D Additional experimental details for curvature

### D.1 Pipeline

Before we visualize the PH pipeline, we give an illustrative figure that provides some intuition on why PH can detect curvature.

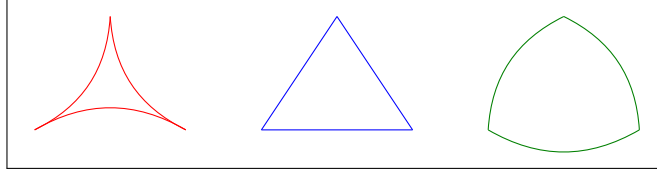


Figure 15: Intuition behind curvature detection with PH. For triangles embedded on a manifold with constant negative (left, in red), zero (middle, in blue) and positive (right, in green) curvature, the length of triangle edges clearly reflect the underlying curvature. Since persistence captures the length of these edges (when the triangle vertices merge into a connected component), PH can be used to detect curvature.

The PH pipeline to detect curvature (Section 4) is visualized in Figure 16. The example point cloud shown in the figure is in the Euclidean plane. We start by calculating the Euclidean distance matrix, and then construct the Vietoris-Rips filtration from these distances, which approximates the point cloud at different scales. 0-dimensional PD registers one persisting cycle reflecting the single connected component of the disk, and many other connected components which have a short lifespan as they get connected to other point-cloud points early in the filtration. There are no persistent 1-dimensional holes since disks are contractible, but there are many holes with short persistence. PDs are then transformed to a vector summary such as a PI.

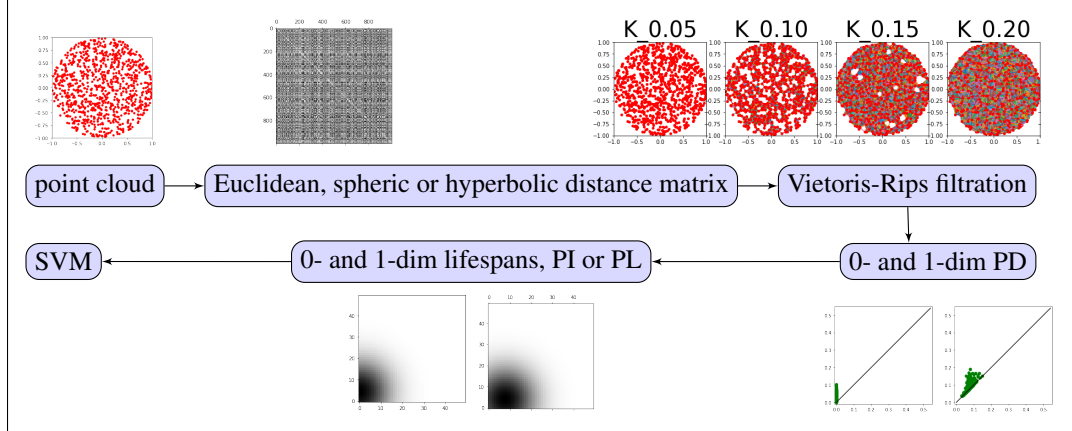


Figure 16: Persistent homology pipeline to detect curvature.

### D.2 Computational resources

Figure 17 visualizes the computational time and memory usage of the different pipelines for this task. The superior performance of the PH pipelines in comparison to other methods (Figure 4) can come at a high cost with respect to the usage of computational resources. The computation times for tuning the standard PH pipelines is comparable to the results for the detection of the number of holes (Appendix C.5), since the PDs consists of similar numbers of persistence intervals, and we consider the same choice of parameters (Appendix B.2). On the other hand, PLs with 10 landscapes are chosen as the best PH signature for the detection of the number of holes, whereas the best signatures for the curvature detection are 0-dim PIs (that do not depend on the number of persistence intervals), and 1-dim PLs with all 292 intervals, yielding a high dimensional PH feature vector.



However, Figure 17 and Figure 4 also show that a small decrease in predictive power and a significant gain with respect to computation time and memory can be achieved with simple PH pipelines that only focus on the lifespans of the PH cycles.

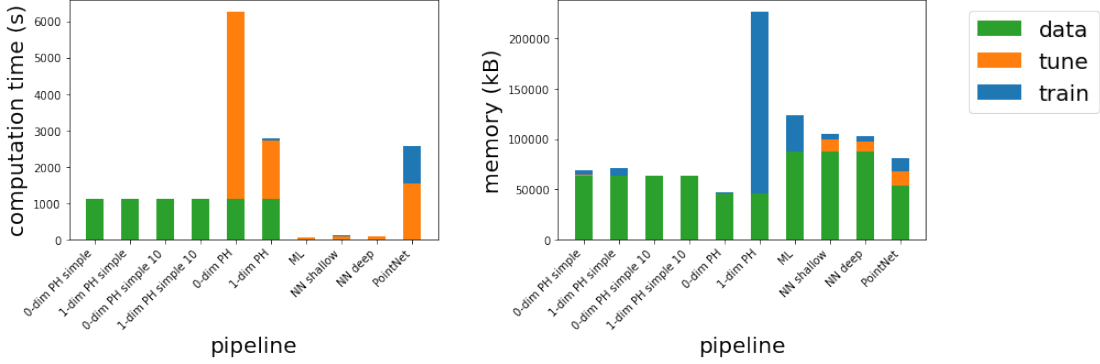


Figure 17: Computational resources for the detection of curvature.

## E Additional experimental details for convexity

### E.1 Pipeline

A visual summary of the PH pipeline used for convexity detection (Section 5) is given in Figure 18. Every shape has at least one 0-dimensional cycle, i.e., connected component. For the given example point cloud, PD with respect to the height filtration from the bottom of the image will have a second persistent connected component. A positive persistence of the second most persisting cycle for at least some direction indicates concavity.

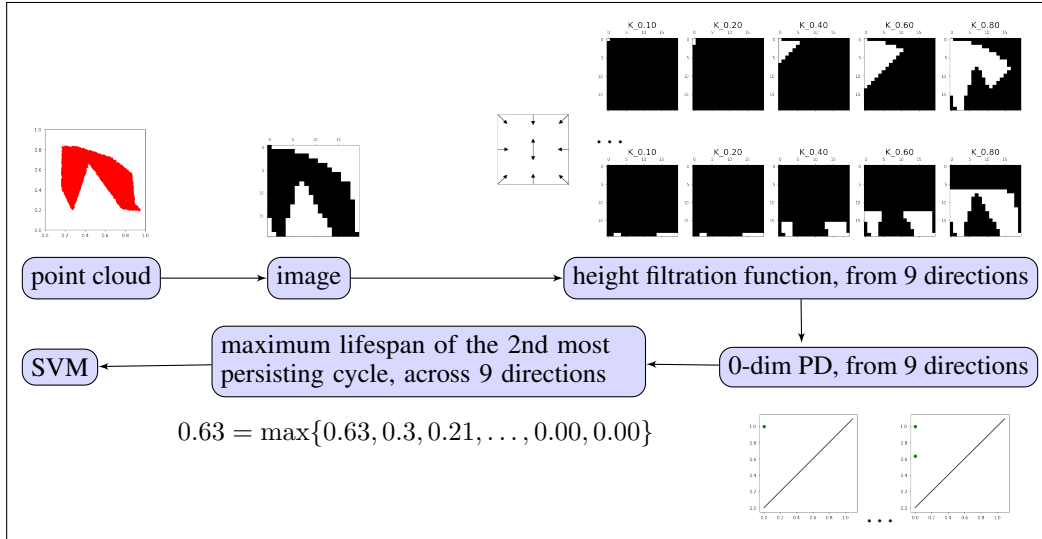


Figure 18: Persistent homology pipeline to detect convexity.

We note here that the convexity could also be detected with PH with respect to the Vietoris-Rips filtration, with some important adjustments. Indeed, [29, Theorem 2] provides a guarantee PH of any function  $f$  and shape  $S$  can be estimated using an algebraic construction based on Rips complexes from a point cloud  $X$  which is a geodesic dense-enough sample of  $S$  (and Theorems 3 and 4 in this paper obtain guarantees in scenarios where both function values and pairwise distances are approximate, i.e., defined on the point cloud). To do so to detect convexity, we cannot employ the standard (so-called vanilla) Vietoris-Rips simplicial complex that relies on the distance function, since

all point cloud points show immediately at  $b = 0$  in the filtration (that all soon get connected into a single component), so that it never sees the two connected components in concave shapes, at any scale  $r \in \mathbb{R}$ , which are captured with cubical complexes. Filtering the point cloud points by their height (yielding a so called weighted Rips filtration) might capture the multiple connected components, but these components can get connected with an edge as soon as they are born, if they are close to each other with respect to euclidean distance (Figure 19). This can be resolved by considering the geodesic distance (the length of the shortest path along the manifold, or a graph), which will allow the multiple connected components to persist longer in the filtration. Indeed, the geodesic distance between points in the “disconnected” regions in concave shapes (the clusters) is larger than the euclidean distance, so that these only get connected later in the filtration.

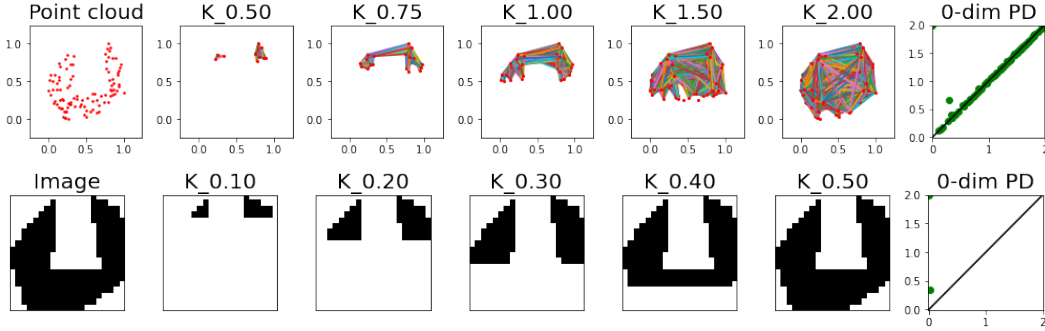


Figure 19: Convexity detection with PH on simplicial and cubical complexes. The concavity can be detected with the weighted Vietoris-Rips simplicial complex, with the filtration function on the vertices defined by height (in this figure, height from the top). The filtration function on edges is defined according to the euclidean distances, but in way that ensures that an edge can only appear in the filtration after both vertices incident to this edge appear in the filtration (for details, see [5]). However, these multiple connected components can still be connected with an edge, if they are close in the euclidean space. This could be circumvented by considering the weighted Vietoris-Rips which relies on the geodesic distances (which are expensive to compute), or by considering cubical complexes instead, where the connected components remain separate until they merge with the rest of the shape.

The important thing to keep in mind is to choose a filtration that will see disconnected components for concave shapes. We choose cubical complexes as they are more straightforward and do not involve the calculation of geodesic distances. Indeed, as the authors of [29] note, geodesic distances are not known in advance and have to be estimated through some neighborhood graph distance, and computing full pairwise geodesic distances is expensive [66, 57] (e.g., there are deep learning efforts to estimate these geodesic distances on point clouds, such as [49, 77].)

## E.2 Computational resources

Results related to the computational efficiency of the different approaches (trained on regular, and tested on regular shapes) are summarized in Figure 20. In this case, the PH pipeline significantly outperforms the other methods, since it relies on a scalar summary of a point cloud (the maximum lifespan of the second most persisting connected component, across 9 height filtration function directions, see Section 5 and Figure 18). On the other hand, PointNet relies on raw point clouds and therefore has a very high memory consumption, since point clouds have 5 000 points for this task (compared to 1 000 points for the detection of the number of holes, or curvature).

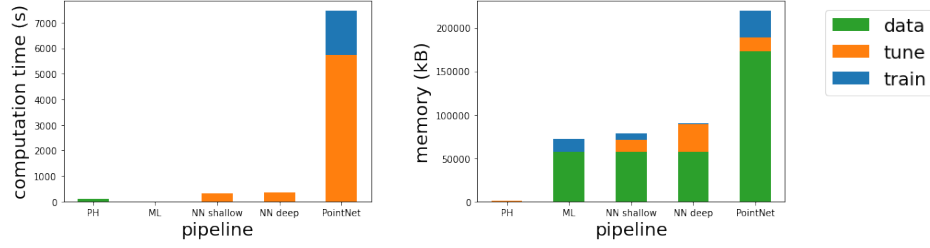


Figure 20: Computational resources for the detection of convexity.

### E.3 Misabeled point clouds

In order to gain a better understanding of the performance and limitations of our PH pipeline, we look at some examples of mislabeled point clouds. Figure 21 shows a few point clouds sampled from concave shapes that are erroneously classified as convex by PH pipeline (trained on regular, and tested on random shapes). The figure also clearly suggests that considering additional directions for the height filtration function would resolve these issues.

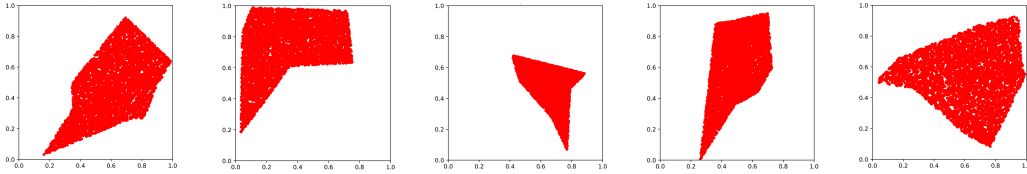


Figure 21: Examples of point clouds from concave shapes incorrectly classified as convex.

## F Guidelines for persistent homology in applications

Our results demonstrate that PH can be successful in applications for which detecting the number of holes, curvature and convexity is important. Based on our findings, we delineate guidelines for the choice of filtrations and signatures, the input and output of PH pipelines, and draw a better understanding of the topology and geometry properties that are captured by long and short persistence intervals (see Figure 22).

We again note here that we use the alpha simplicial complex for the detection of number of holes in order to improve the computational efficiency, but that the same can be done with the standard Vietoris-Rips filtration. In addition, we discuss in Appendix E that convexity can alternatively be detected with the weighted Vietoris-Rips filtration, filtered by height, and relying on geodesic distances.

### F.1 Adjustments of PH pipeline for related applications

Some obvious adjustments to the guidelines from Figure 22 can be made for applications related to the ones that we consider here. Some possible adjustments include the following.

- If it is expected that the dataset is noisy, the suggested filtration function should be weighted by density to achieve robustness to noise (as in Section 3).
- In our experiments, we focused our attention on the PH information relevant to the individual problem at hand, but for other related applications, one might need to consider a different type of information given by PH. For example, if we do not only aim to distinguish between convex and concave shapes, but rather to capture more information about the possibly many concavities, we should not restrict our attention only to the second most persisting cycle, nor consider the maximum across filtration function directions. Instead, it would be useful to take all PH intervals into account for such an application.

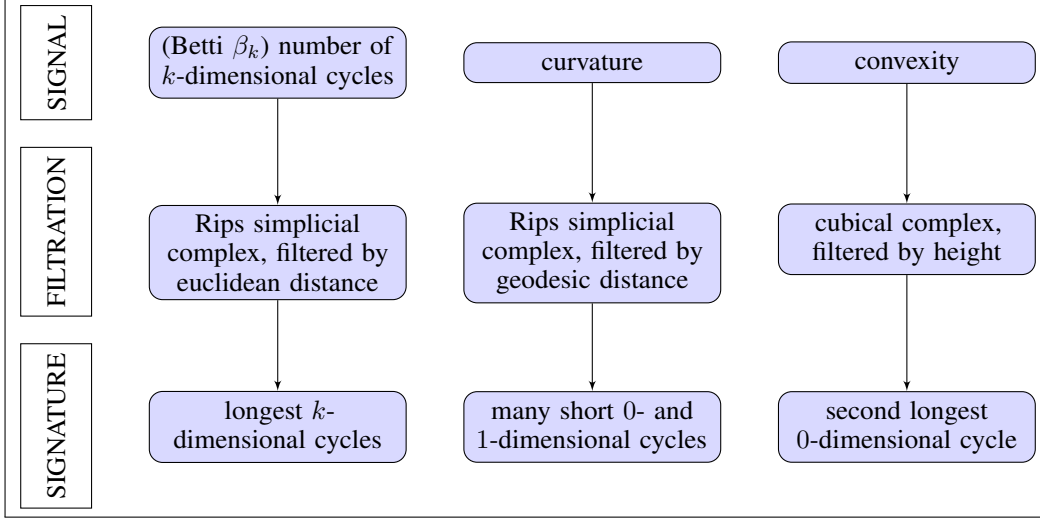


Figure 22: Persistent homology can be useful in applications where  $k$ -dimensional cycles, curvature or convexity are important features. The choice of filtration and persistence signature, including the focus on the long and/or short persistence intervals, depends on the signal of the particular application.

- If there are multiple sources of differences in the data, it can be a good idea to combine the different pipelines. For example, if two classes can be differentiated with some concavities, 0-dimensional persistence on the height filtration will be useful, but if it is also the shape curvature that can help make a distinction, this information can be concatenated with 0- and 1-dimensional PLs on Vietoris-Rips filtration.

## F.2 Discussion of PH pipeline for other applications

**Step 1: Signal** Figure 22 and the discussion above clearly indicate that, when faced with a new problem, it is essential to first try to identify the important information, the signal. To illustrate this more clearly, we list some examples of very different types of signal in Appendix F.2.1, Appendix F.2.2, Appendix F.2.3. Once there is some understanding of the signal, the next steps are to choose the filtration and signature accordingly.

**Step 2: Filtration** The aim is for the filtration to capture the signal. For instance, the Vietoris-Rips filtration encodes the size of cycles, while the height filtration encodes their position. The choice of filtration also influences which type of geometric properties will be captured by long or short persistence intervals. To illustrate the importance of the choice of filtration for the interpretation of long and short intervals, we consider the example point cloud in Figure 9. PH with respect to any meaningful filtration can detect the topology of the underlying shape, i.e., the two holes. However, for the height filtration function from the top of the image, the small circle would have a longer lifespan of the two (as it is born earlier in the filtration), and the large circle can have a seemingly very short lifespan (as it is only born at the bottom of the image). For the Vietoris-Rips filtration it is the opposite (a small cycle has short persistence), and PD on the height filtration from the bottom of the image would see cycles of comparable persistence.

**Step 3: Signature** The choice of persistence signature and the corresponding metric further influences the emphasis on long or short persistence intervals. The Wasserstein distances [20] between PDs place more importance to long persistence, and the same is true for  $L_p$  or  $l_p$  distances between other common choices of persistence signatures, with the standard choice of parameters. However, similarly to our discussion above in F.1, one might want to focus only on short intervals, e.g., by considering only the intervals with lifespan below a certain threshold (so that the distances would be computed between this simplified PH information). Another way to give more weight to short intervals, or intervals of any persistence, is given by an appropriate choice of the weighing function for persistence images. Note, however, that the stability results also depend on the choice of

filtration, persistence signature and metric [95]. Finally, we note that there has recently been a lot of effort in trying to train neural networks to learn what the best PH signature is for specific types of applications [83, 21, 67, 39].

In the remainder of this section, we consider a few hypothetical applications to discuss the relevance of signal, filtration and signature that we hope will be useful for practitioners. In particular, the examples highlight that the importance of long and short persistence intervals depend on the particular application domain. In this context, it is sensible to try to understand the nature of information that is captured with PH (e.g., topological or geometric, any of which might or not be important). The examples thus help us to refine an ongoing discussion in the field about the information detected by intervals of a specific length in a PD:

- **Long persistence intervals as signal.** Indeed, this is true in examples from Figure 23 (when long intervals capture important topology) or Figure 26 (where long intervals capture important geometry). However, an example in Figure 27 (together with results in Section 4 and Section 5) highlights that important information can be encoded in short intervals.
- **Short persistence intervals as noise.** Figure 27 is an example where important information is captured by short intervals (or in this case, a short interval). This can also be seen in the experimental results in Section 4 and Section 5.
- **Long intervals capture topology.** An example in Figure 26 highlights that long intervals, next to topology, also capture geometric information.
- **Many short intervals capture geometry.** An example in Figure 27 (together with results in Section 5) shows that even a single short interval can capture (important) geometry.

### F.2.1 Topology is important, geometry is irrelevant

In some applications, it might be useful to make no distinctions between a circle, a circle with a convex or concave dent, the circle under translation or scaling, or a square (Figure 23). In this case, “shape” is understood through the lens of topology — more precisely, what we are interested in is what is called “homology-type” —, where one object can be deformed into another by bending, shrinking and expanding, but not tearing or gluing. Indeed, to a topologist, a coffee mug and a donut have the same shape.

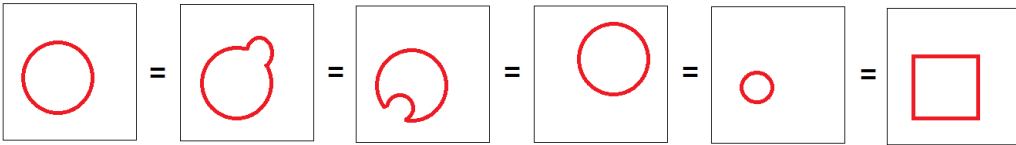


Figure 23: An example of an application where topology is the signal. We consider all the shapes to be the same, i.e., to represent the same class of data, as they all have one connected component and one hole.

It is possible to obtain the same PH summaries for all of the shapes from Figure 23. Indeed, 1-dimensional PDs with respect to the standard Vietoris-Rips filtration on a unit circle and a unit square sampled with same density (reflected in the birth values) could respectively be  $\{(0.1, 1)\}$  and  $\{(0.1, 1.41)\}$ , since the death value reflects the size of the hole. However, we can focus on the cardinality  $|\text{PD}|$  of PDs, that here only encodes topological information. Alternatively, we could rather consider PDs calculated on cubical complexes filtered by the binary or greyscale filtration.

Let us further assume that point clouds with multiple holes might be present in the data, but that the only relevant information is the presence of holes, and not their number (Figure 24). An example of such application could be classification between chaotic and periodic (biological) time series, since the circularity of the so-called Taken’s embedding point cloud reflect periodicity of the underlying time series [74]. In this case, we can only focus on the maximum persistence  $\max\{l = d - b \mid (b, d) \in \text{PD}\}$ . Although PD captures a lot of topology and geometry, this choice of summary obviously ignores a lot of this information.

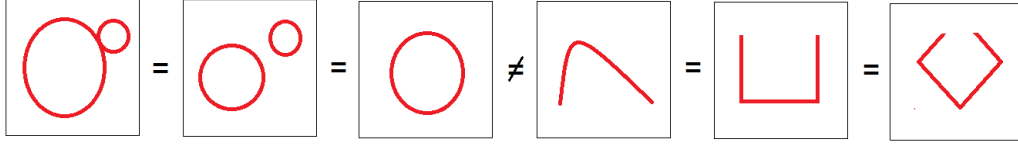


Figure 24: An example of an application where the presence of holes is the signal. The first three shapes in the left part of the figure belong to the same class as there is at least one hole present, whereas the remaining three shapes belong to another class with no holes.

### F2.2 Topology is irrelevant, geometry is important

For other type of applications, the shapes from Figure 23 might be representatives of different classes of objects (Figure 25). Since they all have a single connected component and a single hole, the topological information has no use in discriminating between the classes. However, the geometric information about their size and position is useful.

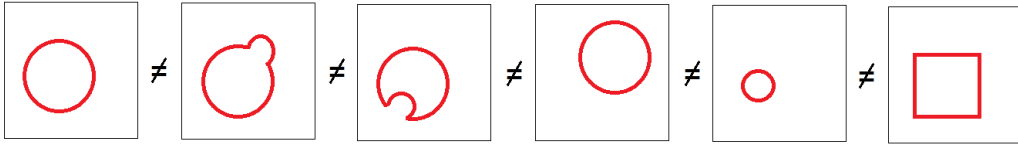


Figure 25: An example of an application where geometry is the signal. In this case, every shape in the figure represents a different object, i.e., they all belong to different data classes.

**Important geometry encoded in long intervals** Consider an example where every shape in the dataset has only two holes (Figure 26), and PH with respect to the Vietoris-Rips filtration. The two longest intervals reflect these two holes (topological information), but their lifespans reflect their size, and it is this geometric signal that can help discriminate between the shapes.

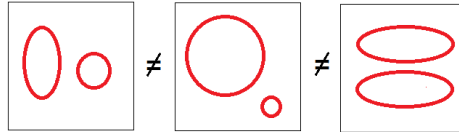


Figure 26: An example of an application where the size of the holes is the signal. The three shapes all have two holes, but their size is meaningful for this application, so that they all belong to different data classes.

**Important geometry encoded in a single interval with the shortest persistence** We consider a hypothetical cancer-detection application. Let us assume that the dataset consists of medical images of some cells in the human body, which look like a certain number of holes (e.g., a grid-like structure). Now imagine that the only difference between the healthy and cancerous cells is the presence of a tiny hole somewhere in the image (which might correspond to some developing cancerous tissue) (Figure 27). For PH with the Vietoris-Rips filtration, the lifespan of each cycle registers its size, but it is the very short persistence of the tiniest holes which would be the most important for this application, as it would be this local geometry signal that would allow to discriminate between the two classes of data, i.e., to detect the presence of cancer.

For example, PH for healthy and cancerous cells can respectively have lifespans  $(20, 20, 20, 20, 0)$  and  $(20, 20, 20, 20, 0.05)$ . The stability theorems imply that the difference between the PH on the healthy and cancerous cells is “small” (or more precisely, it is limited by the difference in their filtrations), but this difference is important for this problem and hence not “noise.”

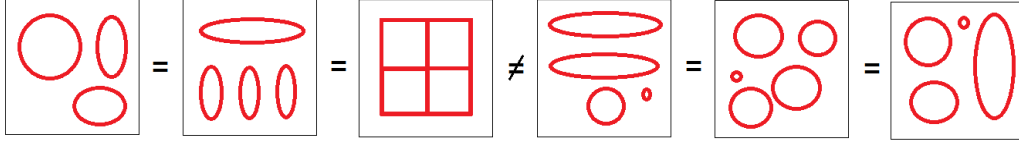


Figure 27: An example of an application where the presence of a tiny hole is the signal. The first three shapes in the left part of the figure reflect the images of healthy cells, whereas the remaining three shapes indicate developing cancerous tissue.

PH can be successful for this task even if the number and size of holes varies across images of healthy cells. In this case, the lifespans for PH of healthy cells could, e.g., be  $(20, 15, 12, 25, 0)$ ,  $(13, 21, 15, 17, 0)$ , and  $(14, 15, 27, 20, 0.05)$ ,  $(19, 21, 15, 17, 0.05)$ , for cancerous cells. Here, the distance between the PH for healthy and cancerous cells is overwhelmed by the distance between the long cycles, that reflect irrelevant information for the problem. However, we could consider a PH signature that only focuses on short intervals, or choose PIs that give a greater weight to short intervals. Alternatively, if there is a number of labeled images available, the difference with respect to the short persistence interval can be learned.

In the same way, it might be the case that images can only be distinguished with a hole of medium persistence, and therefore the importance of different lifespans depends on the application, i.e., dataset. If we know this a priori, we can use PIs and give the greatest weight to the intervals with the most distinctive persistence.

### F.2.3 Topology and geometry are important

To conclude our guidelines, we consider an example of an application in which both geometric and topological information are important. Let us consider a classification problem where the shapes in Figure 28 represent different objects, i.e., different data classes. In this case, it is topology and geometry together that provide useful information. The standard choice of PH on the Vietoris-Rips filtration can help to distinguish between these objects. The PH signature should consider all persistence intervals, since, as discussed in Section 6, geometry (reflecting the size of cycles) is captured in every persistence interval, while the topology is reflected in the number of long-enough intervals.

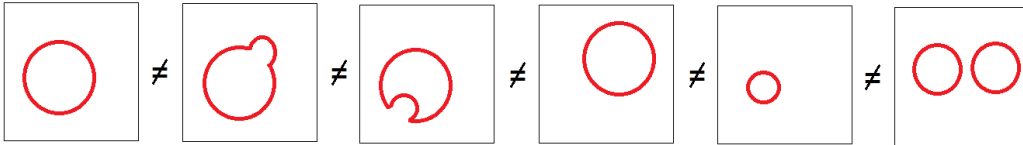


Figure 28: An example of an application where topology and geometry are both signal.

## G Persistent homology detects convexity in FLAVIA dataset

In this section, we employ PH on the FLAVIA dataset which consists of  $1\,907\,1200 \times 1600$  images of plant leaves [105]. Figure 29 shows a few examples of images in this dataset. The goal of these experiments is to show that PH can be effective on real-world data, but also to illustrate the above guidelines about the appropriate choice of filtration and signature for a given application, and the importance of long and short intervals (Appendix F). We focus on convexity detection, as this is the main contribution of our work.

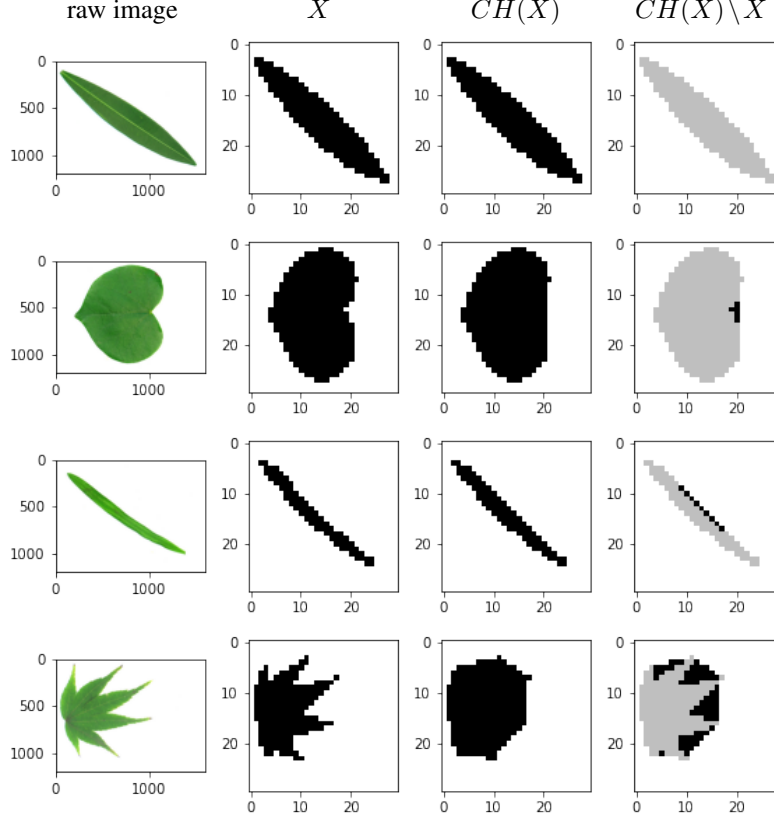


Figure 29: A few example images from the FLAVIA leaf dataset. The images are shown, from top to bottom, with a decreasing label, i.e., convexity measure  $c(X)$ , 1.00, 0.98, 0.89, 0.71. Note that the second image from the top is more convex than the third image, since the considered convexity measure  $c(X)$  is given relative to the area of the leaf. The PH lifespans with respect to the height filtration from 9 different directions from leaf corners and corner center, are respectively from top to bottom, [0.00, 0.00, 0.00, 0.00, 0.00, 0.00, 0.00, 0.00, 0.00], [0.00, 0.00, 0.00, 0.00, 0.00, 0.00, 0.00, 0.00, 0.00], [0.00, 0.00, 1.09, 0.00, 0.00, 0.00, 0.00, 0.00, 0.00], [0.00, 2.52, 10.08, 3.78, 0.00, 1.26, 0.00, 0.00, 0.00].

We classify the leaves according to following measure of convexity which has been shown to be useful for plant species recognition [54]:

$$c(X) = \frac{\text{area}(X)}{\text{area}(CH(X))}, \quad (1)$$

where  $CH(X)$  is the convex hull of image  $X$ . The convexity measure (1) is the most widely used in the literature, and appears in textbooks [114]. Note that we only use the above formula to properly label the dataset (Figure 29), but that, deriving convexity information in such a way involves employing a convex hull algorithm.

In the simpler scenario of a binary classification between convex or concave shapes (i.e., signal is the simple: convex - yes or no), we could rely on the same pipeline as in Section 5, where we consider the lifespan of the second most persisting connected component, and then store the maximum such value across all 9 height filtration directions (Figure 18). This is sufficient information, since we are only interested in whether PH sees multiple connected components - source of a concavity, from *at least one* direction.

However, the convexity measure (1), the signal in our application, provides a more detailed level of information (regression problem), so that we keep the lifespan of the second most persisting connected component *for all* directions, in order to capture information about sources of concavities seen from



any of the directions. Moreover, since the convexity measure is calculated relative to the size of the leaf, the height filtration *directions* remain the same, but the origins change from the 8 corners around the image (Figure 18) to the corners of the leaf; and the lifespans are normalized relative to the area of the leaf (total number of black pixels in the binary image). In this way, PH depicts information about concavities from any direction and relative to the leaf size, and it is invariant under translation and scaling. We use  $30 \times 30$  cubical complexes (on binary images), to capture a higher level of detail for the leaves of different convexity, in comparison with the  $20 \times 20$  resolution for the cruder differences in our synthetic dataset in Section 5. Figure 30 visualizes the height filtration from the 9 different directions, and the resulting 0-dimensional PDs, for an example leaf image (bottom image from Figure 29).

Linear regression on the FLAVIA dataset, trained on 70% of random images, with each image represented with the 9-dimensional vector of lifespans of the second most persisting component across all height filtration directions, obtains a mean square error of 0.00065. The regression line in Figure 31 shows that PH is effective in classifying the FLAVIA leaves according to a measure of convexity. The convexity of some thin leaves (such as the image in the third panel in Figure 29) gets overestimated with our PH pipeline, since concavity is not captured well with our crude resolution, that could easily be improved.

Furthermore, even more detailed information can be captured if the lifespans of the third, fourth, ... most persistent connected component would be kept, because some leaves have more than two sources of concavity from a single direction, that result in more than two connected components. For example, the 0-dimensional PD of the image in Figure 30 has more than two persistence intervals for some height filtration directions. The accuracy can thus be improved by considering the lifespans of *all* short intervals (and across all directions), and again, by considering more height filtration directions (Section 5). This clearly illustrates how the choice of filtration and signature, the input and output of PH, should be guided by the signal in the given application. Moreover, it shows that one short interval can be sufficient for some applications, but that in other cases, many short intervals might store the needed additional level of (geometric) information.

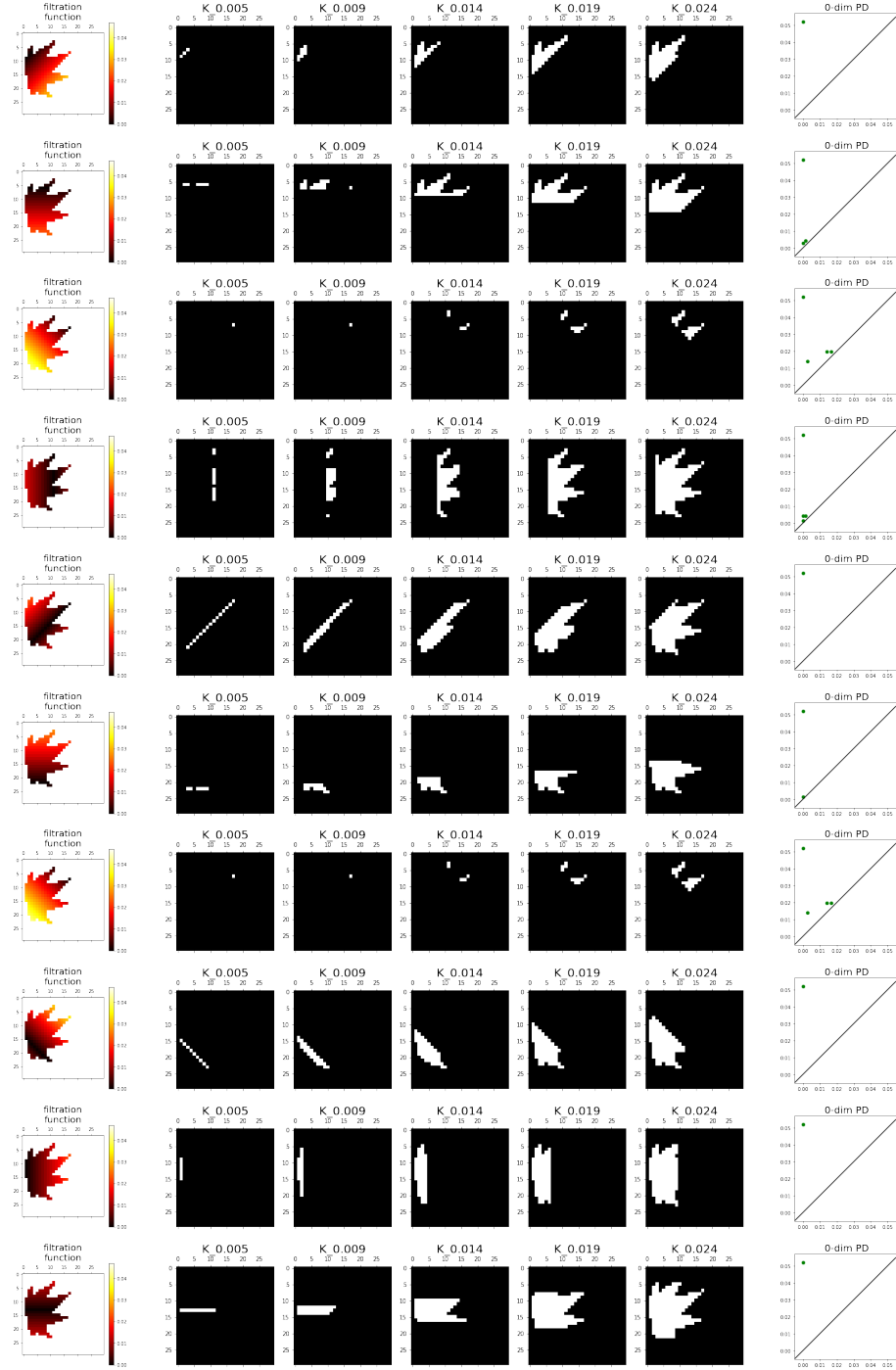


Figure 30: The height filtration from the 9 considered directions, and the resulting 0-dimensional PDs for an example image. The concavity is detected with multiple connected components that are seen from a few directions.

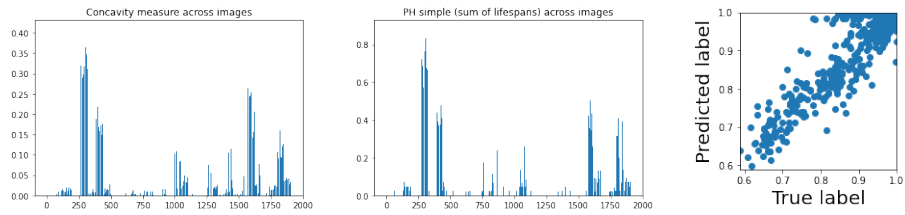


Figure 31: Results on the FLAVIA dataset. The first two plots show that there is a good correspondence between the concavity measure ( $1 - c(X)$ ) (left panel) and the simple PH signature that only considers the sum of lifespans across the height filtration directions (middle panel). The regression line on lifespans from all 9 height filtration directions shows good performance of our PH pipeline.